TAF10 is required for the integrity of TFIID and SAGA complexes but is initially dispensable for somitogenesis in the mouse embryo

Paul Bardot[1,2,3,4,*], Stéphane D. Vincent[1,2,3,4,*,‡], Marjorie Fournier[1,2,3,4,§,#], Alexis Hubaud[1,2,3,4,†,#], Mathilde Joint[1,2,3,4], László Tora[1,2,3,4] and Olivier Pourquié[1,2,3,4,†]

1 Institut de Génétique et de Biologie Moléculaire et Cellulaire, Illkirch, France

2 Centre National de la Recherche Scientifique, UMR7104, Illkirch, France

3 Institut National de la Santé et de la Recherche Médicale, U964, Illkirch, France

4 Université de Strasbourg, Illkirch, France

‡ author for correspondence:

Stéphane. D Vincent (vincent@igbmc.fr)
IGBMC, Development and Stem Cells department
1 rue Laurent Fries
67400 Illkirch
France

*,# equal contributions

present address

§ Sir William Dunn School of Pathology, University of Oxford, Oxford, UK

† Brigham and Woman's Hospital, Boston, USA, Harvard Medical School, Boston, USA

running title: transcription complexes in the embryo

keywords: transcription, embryo, paraxial mesoderm, somitogenesis, SAGA, TFIID

Summary statement

In this study, we characterized the composition of TFIID and SAGA complexes in the mouse embryo and analysed the effect of the depletion of their common subunit TAF10 in the mesoderm.

Abstract

Cell fate and patterning during development are controlled by gene expression. Pre-initiation complex (PIC) formation at promoters is crucial to recruit the transcriptional machinery. The PIC has mainly been studied *in vitro*, and little is known about its composition and function during development. TAF10 is a subunit of TFIID and of the transcriptional co-activator SAGA. Here we characterized TFIID and SAGA's composition during mouse development. Our data indicate that TAF10 is required for TFIID and SAGA assembly. To analyse TAF10-dependent gene regulation during development, we conditionally deleted *Taf10* in the mesoderm. Our results provide evidence for a time window during which *Taf10* loss in the presomitic mesoderm (PSM) does not prevent cyclic gene transcription or PSM patterning while lateral plate differentiation is profoundly altered. During this period, global steady state mRNA levels are not significantly affected in the PSM although the expression of a subset of specific genes is dysregulated. Together, our data demonstrate a differential sensibility of mesodermal tissues to the lack of TAF10. This supports a differential requirement for TAF10 by the general transcriptional machinery during different developmental processes.

(181 words)

Introduction

In mouse, the posterior part of the paraxial mesoderm, called the presomitic mesoderm (PSM), generates a pair of somites every two hours and plays crucial roles during vertebrate elongation (Pourquié, 2011). This rhythmic process is under the control of a clock characterized by periodic waves of transcription of cyclic genes that sweep from the posterior to the anterior of the PSM. In the anterior PSM, the clock signal is converted into a stripe of expression of specific segmentation genes that defines the future somitic domain. The PSM offers a unique paradigm to study transcriptional regulation since it is periodic transcription related to the rhythmic specification of somites occurs.

Gene expression in eukaryotes is the result of the combination of signals such as signalling pathways, which converge towards the binding of transcription factors to regulatory elements and promoters. These interactions lead to the recruitment and assembly of the transcriptional machinery that will transcribe the genomic sequences into RNA. In non-plant eukaryotes, there are three RNA polymerases able to transcribe the genome and among them, RNA polymerase II (Pol II) is responsible for the production of mRNA and some of the non-coding RNAs (Levine et al., 2014).

Transcription initiation requires the assembly of the Pre-Initiation Complex (PIC) that allows the correct positioning of Pol II on the promoter sequence of genes and the consequent RNA synthesis (Sainsbury et al., 2015). Among the general transcription factors that constitute the basal transcription machinery, TFIID is the first recruited to the promoter. In its canonical form in higher eukaryotes, it is composed of TBP (TATA binding protein) and 13 TBP-Associated Factors (TAFs) and it is involved in the correct positioning of Pol II on the transcription start site. While TBP is also part of RNA polymerases I and III transcription complexes, the TFIID-TAFs are specific for Pol II transcription machinery. Among the TAFs,

TAF9, TAF10 and TAF12 are also shared by the SAGA (Spt-Ada-Gcn5-acetyl transferase) complex, a transcriptional co-activator conserved from yeast to human (Spedale et al., 2012). SAGA exerts a HAT activity at the level of the promoters and also deubiquitylates histone H2Bub at the level of gene bodies, suggesting that it acts on transcription initiation but also on gene elongation (Bonnet et al., 2014; Wang and Dent, 2014; Weake et al., 2011).

Several structural TAFs, including TAF10, are characterized by the presence of a Histone Fold Domain (HFD) involved in their dimerization with specific partners. In particular, the TAF10 heterodimerizes with TAF3 or TAF8 within TFIID and with SUPT7L/ST65G within SAGA (Leurent et al., 2002; Soutoglou et al., 2005). Heterodimerization is required for TAF10 nuclear import since it does not have a nuclear localization signal (NLS) (Soutoglou et al., 2005).

TAF10 does not exhibit any enzymatic activity but serves as an interface allowing interaction with other TAFs (Bieniossek et al., 2013; Trowitzsch et al., 2015) or some transcriptional factors such as human estrogen receptor α (Jacq et al., 1994) or mouse GATA1 (Papadopoulos et al., 2015). Only 50% of the TFIID complexes contain TAF10 in HeLa cells (Jacq et al., 1994). A lower proportion of TFIID complexes lacking TAF10 has also been observed in F9 cells (Mohan et al., 2003), but the functionality of these complexes remains to be addressed. Altogether, these data support the idea that TFIID composition can vary, as also suggested by the existence of TAF paralogs and/or tissue specific TAFs (Goodrich and Tjian, 2010; Müller et al., 2010).

The diversity in the composition of the TFIID complexes may have functional consequences. Whereas TAF10 is crucial for survival and proliferation of F9 teratocarcinoma cells, it is dispensable for their RA-induced differentiation into primitive endoderm (Metzger et al., 1999). The null mutation of *Taf10* in mouse leads to embryonic lethality shortly after implantation (Mohan et al., 2003). Interestingly, while inner cell mass dies by apoptosis,

trophoectodermal cells survive, although Pol II transcription is greatly reduced in these cells (Mohan et al., 2003). Conditional deletion of *Taf10* in skin or liver has shown that TAF10 is required for transcription in the embryo but can be dispensable in adult tissues (Indra et al., 2005; Tatarakis et al., 2008). Altogether, these data clearly show that TAF10 requirement depends on the cellular and developmental context.

The structure of the TFIID complex in the absence of TAF10 is unclear. Only partial TFIID sub-complexes, not associated with TBP, were detected in undifferentiated and RA-differentiated *Taf10* mutant F9 cells (Mohan et al., 2003), while complete disruption of TFIID was observed in *Taf10* mutant liver cells (Tatarakis et al., 2008). The integrity of the SAGA complex was not investigated in detail in these experiments (Mohan et al., 2003; Tatarakis et al., 2008).

In this study, we aimed to closely analyse TAF10 requirement and its role in transcription during mouse development and to look precisely at the composition of TFIID and SAGA in the absence of TAF10 in embryonic tissues *in vivo*. In order to do so, we performed immunoprecipitations coupled to mass spectrometry analyses on embryonic lysates. Our results show that the assembly of TFIID and SAGA complexes is strongly affected in the absence of TAF10. In order to get more insight into the functional importance of TAF10 during development, we focused on the dynamic differentiation of the paraxial mesoderm by carrying out a conditional deletion of *Taf10* in the mesoderm using the *T-Cre* transgenic line (Perantoni, 2005). Loss of *Taf10* leads to a growth arrest and to the induction of cell death around E10.5. However, we identified a time window during which the dynamic transcription of cyclic genes is still maintained in the absence of TAF10 protein. Microarray analysis of mutant PSM revealed that Pol II transcription is not globally affected in this context, although expression of some genes, such as genes encoding cell cycle inhibitors, is up regulated.

Results

TAF10 is ubiquitously expressed in the nucleus of embryonic cells at E9.5

Taf10 is ubiquitously expressed in the mouse embryo at E3.5, E5.5 and E7.5 but with more obvious heterogeneity at E12.5 (Mohan et al., 2003). *W*hole-mount *in situ* hybridization analyses suggest that *Taf10* is also ubiquitously expressed at E8.5 and E9.5 (Fig. S1A,B). TAF10 protein is ubiquitously expressed in the posterior part of the embryo (Fig. S1C, Fig. S2) and no heterogeneity was observed between E9.5 and E10.5. Competition with the peptide used to raise the anti-TAF10 antibody (Mohan et al., 2003) confirms that TAF10 localization is specific since the TAF10 signal, but not the Myogenin signal, is lost in these conditions (Fig. S1D,H). Altogether these results indicate that between E8.5 and E10.5, TAF10 protein is expressed in cell nuclei in the mouse embryo.

Induced ubiquitous deletion of *Taf10* leads to growth arrest at E10, but does not impair transcription at E9.5

In order to analyse the effects of TAF10 absence on mouse development, we performed an inducible ubiquitous deletion of *Taf10* using the $R26^{CreERT2}$ line (Ventura et al., 2007). This strategy deletes the exon 2 of *Taf10* that encodes for part of the HFD (Mohan et al., 2003). Since *Taf10* exon 3 is out of frame, this deletion potentially produces a truncated protein of 92 amino-acids (Fig. S3) that does not contain the crucial HFD for heterodimerization and integration of the protein into TFIID and SAGA complexes (Leurent et al., 2002; Soutoglou et al., 2005). Tamoxifen was injected intraperitoneally at E7.5 and Cre recombination was followed by the activity of the Cre reporter allele $R26^{R}$ (Soriano, 1999). As shown in Fig. 1A,B, Cre recombination is very efficient at E9.5. The development of $R26^{CreERT2/+}$;$Taf10^{flox/flox}$ (referred after as *R26Cre;Taf10*) mutant embryos is arrested at E9.5 since they do not evolve when recovered at E10.5 and E11.5 (Fig. 1D and F, respectively).

The normal development of *R26*$^{R/+}$;*Taf10*$^{flox/flox}$ embryos littermates (Fig. 1C,D) confirmed that tamoxifen injection at E7.5 does not induce secondary defects in our model. Loss of TAF10 protein at E9.5 after tamoxifen injection at E7.5 was confirmed by western blot analysis (Fig. 1G).

In order to assess transcription initiation *in vivo*, we took advantage of the transgenic line *Luvelu* (Aulehla et al., 2008) that allows visualization of the dynamic waves of *Lfng* transcription occuring every 2 hours in the posterior PSM. This line contains the promoter and 3' UTR destabilizing sequences of the cyclic gene *Lfng* (Cole et al., 2002; Morales et al., 2002), coupled to the coding sequences of a Venus-PEST fusion. *Luvelu* expression is not affected in the absence of TAF10 at E9.5 clearly supporting the idea that transcription initiation still occurs in the *R26Cre;Taf10* mutant embryos, at least in the PSM (Fig. 1H,I).

Altogether, these results indicate that we have identified a time window around E9.5 during which deletion of *Taf10* is effective but gene expression is not globally affected.

Analyses of the composition of the TFIID and SAGA complexes in absence of TAF10 in the mouse embryo

Next we set out to analyse the composition of TFIID and SAGA complexes in the E9.5 mouse embryo, at a time point when TAF10 protein is not detected, but when transcription is still operational (see above). To purify TFIID and SAGA complexes, we collected E9.5 embryos from *R26*$^{CreERT2/CreERT2}$;*Taf10*$^{flox/flox}$ x *Taf10*$^{flox/flox}$ crosses, treated (mutant) or not (control) with tamoxifen at E7.5. Efficient deletion of *Taf10* was assessed by PCR (data not shown) and absence of detectable full-length TAF10 protein was confirmed by western blot analysis (Fig. 2A). Interestingly, expression of TBP, TAF4A, TAF5 and TAF6 is not affected in absence of TAF10, whereas expression of TAF8, the HFD-containing partner of TAF10, is strongly decreased (Fig. 2A).

We then assessed TFIID and SAGA composition by performing immunoprecipitations (IPs) against different TFIID and SAGA subunits with anti-TBP or anti-TAF7 antibodies (for TFIID) and with anti-TRRAP or anti-SUPT3 (for SAGA). To be able to compare control and *Taf10* mutant samples, we calculated the normalized spectral abundance factor (NSAF) (Zybailov et al., 2006).

In mass spectrometry analyses of control embryos, the full-length TAF10 protein is represented by 4 peptides (Fig. S4A). In the mutant embryo samples, no TAF10 peptides were detected in the TBP- and TRRAP-IPs. In contrast a few peptides were recovered in both TAF7- and SUPT3-IPs. Surprisingly, when we scored the distribution of the detected peptides in either the TFIID- or the SAGA-type IPs, we observed a striking difference in the pattern of detected peptides in mutant embryos for TAF7- and SUPT3-IPs where there is a clear bias toward the detection of peptide #1 (Fig. S4B,C). This suggests that a potential short truncated TAF10 protein (Fig. S4D), lacking the HFD, corresponding to exon 1 fused to exon 3 which becomes out of reading frame introducing a stop codon, may be detected in the mutant samples. Thus for further analyses and to score only the full-length protein, we took into account peptides #2 to #4 that should be absent from the full-length TAF10 protein after deletion of the genomic sequences (TAF10*, Fig. 2D and Fig. 3C, and Fig. S4A,C) for TAF7 IPs (Fig. 2D) and SUPT3 IPs (Fig. 3C). Data for TAF7 and SUPT3 IPs taking into account all the TAF10 peptides are shown in Fig. S5.

TBP is also part of other complexes; SL1 and TFIIIB, involved in Pol I and Pol III transcription, respectively (Vannini and Cramer, 2012). Importantly, the absence of TAF10 does not perturb the interaction of TBP with its non-TFIID partners, highlighting the lack of non-specific effect (Fig. 2B). In *Taf10* mutant embryos, we even observed an increase in the interaction between TBP and the larger subunits of SL1; TAF1A and TAF1C, suggesting that TBP may be redistributed in Pol I TAF-containing complexes in absence of TAF10 as it has

been previously shown that there is no free TBP in the cells (Timmers and Sharp, 1991). In control TBP- and TAF7-IPs, all the canonical TFIID subunits were detected (Fig. 2C,D). Interestingly, in *Taf10* mutant embryos, TBP IP reveals that TBP is mostly disengaged from the TFIID complexes as only a few TAFs co-immunoprecipitate with TBP in much lower amounts (Fig. 2C). This TFIID dissociation is also observed in the TAF7 IP in absence of TAF10 (Fig. 2D). Surprisingly however, due to the very efficient TAF7 IP (Table S1), we can still detect residual canonical TFIID complexes as TAF10 peptides corresponding to the full-length protein were also detected in mutant embryos (Fig. 2D).

In order to assess SAGA composition, we performed IPs against two of its subunits: SUPT3 and TRRAP. TRRAP is also a member of the chromatin remodelling complex TIP60/NuA4 (Sapountzi and Côté, 2011). As the interactions between TRRAP and TIP60/NuA4 subunits were not affected (Fig. 3A), we concluded that TAF10 absence does not interfere with the interactions between TRRAP and its non-SAGA partners. In both mutant TRRAP (Fig. 3B) and SUPT3 (Fig. 3C) IPs, we observed a dramatic defect in the assembly of the SAGA complex. Contrary to TAF7 IP, we were not able to detect any residual canonical SAGA complexes in the mutant samples.

Altogether, these results strongly suggest that TAF10 is crucial for the assembly of both TFIID and SAGA complexes in the mouse embryo, since the formation of both complexes is seriously impaired in *R26Cre;Taf10* mutant embryos. Our data also suggest that in *R26Cre;Taf10* mutant embryos, a truncated form of TAF10 protein lacking a HFD is synthesized and can be incorporated, albeit less efficiently, into TFIID or SAGA-like complexes.

Conditional deletion of *Taf10* in the paraxial mesoderm

Somitogenesis is a very dynamic developmental process in vertebrate embryos that relies on periodic transcriptional waves sweeping from posterior to anterior in the PSM

(Hubaud and Pourquié, 2014). To investigate the role of TAF10 in the this process, we carried out a conditional deletion of *Taf10* in the PSM using the *T-Cre* transgenic line (Perantoni, 2005). This line expresses Cre under the control of 500-bp *T* promoter sequences (Clements et al., 1996) leading to efficient recombination in the mesoderm prior to E7.5, including in paraxial mesoderm progenitors (Perantoni, 2005). It is not guaranteed that the composition of TFIID and SAGA complexes in the mesoderm is similar to the average of whole embryos, but it is very likely that absence of TAF10 has a similar effect on the assembly of these complexes. Conditional deletion of *Taf10* is embryonic lethal as no *T-Cre*/+;*Taf10*$^{flox/flox}$ mutants (referred after as *T-Cre;Taf10* mutants) could be recovered at birth (data not shown). At E9.25, control and *T-Cre;Taf10* mutant embryos are very similar (Fig. 4A,B). At E10.25, *T-Cre;Taf10* mutant embryos exhibit normal anterior development but show an apparent growth arrest of the trunk region. These mutants present a helicoidal trunk and tail, as well as an absence of limb buds (Fig. 4C,D) and a degeneration of the allantois and placenta (data not shown). Whereas at E9.25 mutant and control somites were similar (Fig. 4A,B), E10.25 mutant somites were much smaller (Fig. 4C,D). Similar observations were made using the *Hes7-Cre* deleter strain (data not shown) that has a similar recombination pattern in the mesoderm (Niwa et al., 2007). Lysotracker Red staining indicates that there is no obvious cell death in the mutants at E9.25 (Fig. 4E,F). Recombination is efficient as shown by the profile of activation of the Cre reporter allele *R26*^{R} at E8.75 (Fig. 4G,H). In order to rule out the persistence of TAF10 protein in *T-Cre;Taf10* mutant embryos, we analysed TAF10 expression. Expression of TAF10 was mosaic in the mutant neural tube (NT) as the late streak and the tail bud contain bipotent neuro-mesodermal progenitors (Gouti et al., 2014; Tzouanacou et al., 2009). As shown in Fig. 4J,L compared to Fig. 4I,K, a full-length TAF10 protein could not be detected in the mesoderm of mutant embryos, including the PSM, but was maintained in the ectoderm. Surprisingly, these data show that there is a time window

around E9.5 when embryonic development is not affected upon TAF10 protein depletion, prior to an apparent growth arrest and decay at E10.5.

Absence of TAF10 in the PSM does not affect somitogenesis

To further characterize these somitogenesis defects, we quantified the somite index by calculating the number of somites per embryo subtracted by the average number of somites of the whole litter at E9.5. We could not identify any statistically significant difference in somite index among the different genotypes (Fig. 5A). We next analysed the expression of specific PSM markers using whole-mount *in situ* hybridization. Expression of the posterior PSM marker *Msgn1* (Wittler et al., 2007) (Fig. 5B,C), of the clock downstream target *Mesp2* (Saga et al., 1997) (Fig. 5D,E) or of the caudal somite marker *Uncx4.1* (Neidhardt et al., 1997) (Fig. 5F,G) is not affected in absence of TAF10. Whole-mount *in situ* hybridization of cyclic genes of the Notch (*Hes7* (Bessho et al., 2003) and *Lfng* (Forsberg et al., 1998; McGrew et al., 1998), Fig. 5H,I and S5A,B), Wnt (*Axin2* (Aulehla et al., 2003), Fig. S6C,D) or FGF (*Snai1* (Dale et al., 2006), Fig. S6E,F) signalling pathways revealed that the different phases of expression could be observed in *T-Cre;Taf10* mutant embryos. Altogether, the rhythmic transcription of the cyclic genes in absence of TAF10 suggests that active transcription proceeds normally in the PSM of mutant embryos.

Absence of TAF10 differentially affects the mesoderm derivatives

Limb bud outgrowth requires signals such as *Fgf8* from the Apical Ectodermal Ridge (AER) which controls proliferation of the underlying mesenchyme derived from the lateral plate mesoderm (Zeller et al., 2009). On E10.25 transverse sections from control embryos, mesodermal nuclei (including in the paraxial and lateral (LPM) plate mesoderm) are regularly shaped (Fig. 6A,C,E). However, in *T-Cre;Taf10* mutants (Fig. 6B), the paraxial mesoderm nuclei appear normal (Fig. 6D) while in the LPM (and in the intermediate mesoderm (data not shown)), massive nuclear fragmentation characterized by the presence of pyknotic nuclei is

detected (Fig. 6F). These data suggest that the LPM is more sensitive to the loss of *Taf10* than the paraxial mesoderm.

We carried out whole-mount *in situ* hybridization in order to test whether *Taf10* loss differentially affects the expression of specific markers of the different types of mesoderm. Expression of the LPM marker *Hand2* (Fernandez-Teran et al., 2000) is clearly diminished in absence of TAF10 (Fig. 6G,H). Similar observations were made with *Prdm1* that is expressed in the growing mesenchyme during limb bud outgrowth (Vincent et al., 2005) (data not shown). The absence of *Fgf8* induction in the presumptive AER in E9.5 *T-Cre;Taf10* mutant embryos (Fig. 6K,L) indicates that the LPM defect is early and probably precedes the cell death in this tissue since no obvious cell death could be detected at E9.25 (Fig. 4F). The cell death observed later on in the LPM is however not caused by the lack of *Fgf8* expression as it is also observed at non-limb levels. In contrast, analysis of paraxial mesoderm markers shows that *Pax3* expression in the anterior PSM and early somites (Goulding et al., 1991) is normal (Fig. 6I,J). Similarly, the expression domains of *Fgf8* in the rostral and caudal lips of the dermomyotome (Crossley and Martin, 1995) are not affected at E9.5 by the absence of TAF10 in the paraxial mesoderm (Fig. 6 K,L). Expression of *Pax3* in the dermomyotome (Goulding et al., 1991) and of *Myf5* in the myotome (Ott et al., 1991) is however decreased in the *T-Cre;Taf10* mutants (Fig. 6M,N). Delayed myotome formation was evidenced by immuno-localization of Myogenin or Myosin Heavy Chains at E9.5 and E10.5 (data not shown). Similar observations were made in *Hes7-Cre;Taf10* mutant embryos (Fig. S7). Expression of *Shh* in the notochord is normal (Echelard et al., 1993) indicating that the axial mesoderm is not obviously affected in the *T-Cre;Taf10* mutant embryos (Fig. 6O,P). Altogether, these results indicate different requirements for TAF10 depending on the type of mesoderm.

The absence of TAF10 does not affect global steady state mRNA and cyclic transcription in the PSM

Our next goal was to investigate Pol II transcription status in mutant embryos. We first compared steady state rRNA (Pol I) and mRNA (Pol II) transcript levels by quantifying the absolute expression levels of *RNA18S* (3 primer pairs) versus classical Pol II house keeping genes (*Actc1*, *Gapdh* and *Rplp0*) (Fig. 7A). No significant differences between mutant and control samples were detected when comparing the results obtained with 3 different pairs of RNA 18S primers (Fig. 7B). The results are similar for *Gapdh* and *Rplp0* (Fig. 7B).

Expression of the *Luvelu* reporter(Aulehla et al., 2008) in *T-Cre;Taf10* mutant embryos (Fig. 7C,D) supports the idea that cyclic transcription initiation still occurs in the *T-Cre;Taf10* mutant PSM. Altogether these results indicate that, around E9.5, in the absence of detectable TAF10, global steady state mRNA and PSM-specific cyclic transcription are not affected.

Expression of specific genes is altered in the PSM at E9.5 in the absence of TAF10

We next performed a transcriptome analysis in order to see whether specific genes were affected in absence of TAF10. We performed microarray analyses from micro-dissected PSMs of 17-19 somites control and *T-Cre;Taf10* mutant embryos (Fig. 8A). Analysis of the microarray by scatter plot shows that loss of TAF10 has only very minor impact on gene expression (Fig. 8B). We then performed a statistical analysis using Fold Change Ranking Ordered Statistics (FCROS) (Dembélé and Kastner, 2014). We found 369 differentially expressed genes using a fold change cut-off of 1.5x (218 down-regulated and 151 up-regulated, see Supplementary Table 2). This analysis identified genes related to the cell cycle, TAFs, signalling pathways components, or *Hox*/*para-Hox* genes (see Table 1). We also observed that some genes previously identified as cyclic genes in the PSM such as *Egr1*, *Cyr61*, *Dkk1*, *Spry4* and *Rps3a* (Krol et al., 2011), are also differentially expressed in the *T-*

Cre;Taf10 mutant PSMs (Table 1 and Fig. S8A). Interestingly, the highest up-regulated gene (4.8 fold) is *Cdkn1a* that encodes a cyclin-dependent kinase inhibitor that induces a G1 arrest (Dulić et al., 1994). We also identified *Gas5*, a tumor suppressor gene that encodes 2 lncRNAs and several small nucleolar RNAs in its introns (Ma et al., 2015) as the highest down-regulated gene (from -2 to- 4.9 fold). We confirmed the up-regulation of *Cdkn1a*, *Cdkn1c*, *Ccng1* and *Cdkl3*, and the down-regulation of *Gas5* by RT-qPCR using control and *T-Cre;Taf10* mutant tail tips (Fig. 8D). Up-regulation of *Cdkn1a* and *Cdkn1c* could explain the growth arrest that is observed in the *T-Cre;Taf10* mutant embryos.

Among the up-regulated genes, we also found TFIID-TAFs: *Taf5* (1.5 fold), *Taf6* (1.7 fold) and *Taf9b* (1.6 fold) (Table 1, Table S2). We validated these differential expressions by RT-qPCR and found that the expression of most of the genes encoding for the other TAFs were also up-regulated (Fig. S8B). The biological significance of these differences is not clear as no obvious increase in protein levels could be observed for TAF4A, TAF5 and TAF6 (Fig. 3A). *Taf10* expression is down-regulated in *T-Cre;Taf10* mutant tail tips and expression of *Taf8*, encoding TAF10's main TFIID partner is also down-regulated in the mutant condition. These data suggest that the decreased level of TAF8 protein observed in *R26Cre;Taf10* lysates (Fig. 2A) could also be related to a transcriptional regulation. We also checked the expression level of genes coding for TAF subunits of the SAGA complex, including the SAGA-specific TAF5L and TAF6L, but could not see any significant differences (Fig. S8C). Altogether, our data show that gene expression controlled by Pol II is not initially globally affected in the absence of TAF10, however, the lack of TAF10 could induce a change in the steady state mRNA levels of specific genes.

Discussion

The composition of TFIID and SAGA complexes in the developing embryo has not been investigated. Here, we analysed the composition of these complexes in E9.5 mouse embryos in presence and absence of TAF10. We showed that both TFIID and SAGA complexes formation is strongly affected in absence of TAF10. Deletion of *Taf10* during somitogenesis confirmed the requirement of TAF10 during embryonic development in agreement with previous studies (Indra et al., 2005; Mohan et al., 2003; Tatarakis et al., 2008). However, in contrast to these studies, we identified a time window around E9.5 when no obvious somitogenesis defects are detected, despite the absence of detectable full-length TAF10 protein in mutant embryos. In these mutant embryos, transcription is still functional as shown by the lack of global effect on RNA polymerase II transcription.

TAF10 is required for TFIID and SAGA assembly during development

Our data demonstrate a global decrease in the assembly of TFIID and of SAGA complexes in the *Taf10* mutant mouse embryos. In F9 cells, in absence of TAF10, the TFIID complex is minimally affected by the release of TBP from the complex, while interaction between the different TAFs is maintained (Mohan et al., 2003) and in the liver, the assembly of TFIID is completely abrogated (Tatarakis et al., 2008). These differences could be explained either by cell-type specific differences or by difference in the timing of these analyses following *Taf10* deletion as Tatarakis *et al*. (2008) performed their experiments 8-15 days after *Taf10* deletion. Our new data show that the defect in the assembly of TFIID is observed already 2 days after the induction of *Taf10* deletion. On the other hand, we can still detect reduced interactions between TAF7 and most of the TAFs following *Taf10* deletion suggesting that, as observed in HeLa or F9 cells, there could be some TFIID-like complexes that do not contain TAF10, albeit in reduced levels.

TAF10 depletion is very efficient since we cannot detect TAF10 proteins by western blot in the mutant embryo lysates. Analysis of the frequency of the detected peptides strongly

suggests that only in this TAF7 TFIID IP, potential full-length TAF10 proteins are detected, albeit at very low frequency. This suggests that very low levels of canonical TFIID complexes could still be present at this stage. Furthermore, these results, in comparison with the anti-SAGA IPs, suggest that TAF10 is very stable when incorporated into TFIID, probably because of the lower rate of TFIID turnover compared to that of SAGA. While existence of such residual TFIID complexes could account for the mild phenotype observed in the paraxial mesoderm, it cannot explain the strong effect of the deletion on LPM derivatives. The status of SAGA has not been previously investigated in *Taf10* mutant embryos. Our work demonstrates that not only TFIID but also SAGA is affected in *Taf10* mutant embryos. TFIID is built from sub-modules, at least *in vitro* (Bieniossek et al., 2013; Trowitzsch et al., 2015), so we cannot exclude that such TFIID sub-modules are also immunoprecipitated in our experiments. Our data however clearly show that while some TAF paralogs, such as TAF4A and TAF4B, TAF9 and TAF9B are present in the mouse TFIID IPs, this is not the case for TAF7L that has been associated with germ cells and adipocytes (Zhou et al., 2013a; Zhou et al., 2013b). This indicates that the majority of TFIID contains TAF7, at least at E9.5. This potential TFIID diversity could exist inside all the cells or could be cell specific. This could explain the developmental differences observed between lateral plate and intermediate mesoderm on one hand, and paraxial mesoderm, on the other hand.

A TAF10 truncated protein can potentially be integrated into TFIID and SAGA complexes

An unexpected observation is the detection of potential residual truncated TAF10 proteins in the *Taf10* mutant condition. Indeed, our strategy conditionally removes exon 2 and theoretically leads to the splicing of exon 1 to exon 3 (Mohan et al., 2003). These exons are not in frame and therefore, the 77 amino-acids coded by exon 1 are followed by 15 extra amino-acids in the mutant (Fig. S5D). The anti-TAF10 antibody 6TA2B11 that was used to detect TAF10 in western blot analyses was raised against a peptide coded by exon 2 (Mohan

et al., 2003), therefore it cannot detect the truncated protein. This mutant protein has the N-terminal unstructured domain of TAF10 and more importantly, does not have its HFD. The HFD is required for the interaction with TAF3, TAF8 or SUPT7L/ST65G (Soutoglou et al., 2005). HFD-HFD interactions are crucial for TAF10 nuclear import which does not contain any NLS (Soutoglou et al., 2005), and thus how this truncated protein can be incorporated in immunoprecipitated SAGA and TFIID complexes is unclear. Nevertheless, the association of this truncated TAF10 peptide with the immunoprecipitated complexes seems relatively stable, as the IPs are washed with high salt buffers. It is also possible that this truncated protein is only incorporated into sub-modules or building blocks that are not fully assembled into canonical complexes.

Another interesting question is the functionality of these potentially partial TFIID and SAGA complexes fully depleted of TAF10 protein or containing the truncated TAF10 protein. From our data, it is obvious that these different partial complexes cannot fully compensate for the loss of wild type complexes, but one cannot rule out a partial activity. Future analyses of the difference between the different types of mesoderm could help to elucidate whether such partial non canonical TFIID and/or SAGA complexes have activities.

Differential sensitivity to the loss of Taf10 in the mesoderm

Deletion of *Taf10* in the mesoderm or in the whole embryo leads to an obvious growth arrest that could be explained by the up-regulation of *Cdkn1a* and *Cdkn1c* expression. Similar observations were made in yeast (Kirschner et al., 2002) and in F9 cells (Metzger et al., 1999), following depletion of TAF10. Surprisingly, we also observed the down regulation of the tumour suppressor *Gas5* that is associated with increased proliferative and anti apoptosis in cancer cells (Pickard and Williams, 2015). Interestingly, it has been established that *Cdkn1a* expression is positively controlled by *Gas5* in stomach cancer at the transcript and

protein levels (Liu et al., 2015). It is thus possible that TAF10 is required for the correct functioning of the *Gas5* regulatory network during development.

The phenotypes of null mutations of TFIID-TAFs genes such as *Taf7* (Gegonne et al., 2012) or *Taf8* (Voss et al., 2000) are very similar to the *Taf10* null phenotype (Mohan et al., 2003). In particular, these mutations are all embryonic lethal around implantation stage. Moreover, *Taf7* null MEFs stop proliferating, suggesting that the growth arrest we observed in our mutants is a direct consequence of the failure to properly build TFIID. We cannot exclude a potential contribution of the loss of the SAGA complex in our mutants. However, deletion of the genes coding for different enzymatic activities of SAGA such as *Kat2a*;*Kat2b* or *Usp22* are embryonic lethal, but with phenotypes much less severe than *Taf10* mutation (Lin et al., 2012; Xu et al., 2000; Yamauchi et al., 2000). Interestingly, axial and paraxial mesoderm formation is affected in *Kat2a*;*Kat2b* mutants whereas, extra-embryonic and cardiac mesoderm formation is not (Xu et al., 2000), strongly suggesting that SAGA could also have different functions in different types of mesoderm.

A striking observation is the difference of sensitivity to the loss of *Taf10* between the LPM (and the intermediate mesoderm) and the paraxial mesoderm. Interestingly, we observed a very early defect in the LPM with the strong down-regulation of specific markers and the absence of limb bud outgrowth. The absence of limb buds could be explained by a defect in FGF10 signalling activation in the mesoderm and/or by cell death in the LPM that occurs earlier than in the paraxial mesoderm of *T-Cre;Taf10* mutants. The relative resistance of the mutant paraxial mesoderm to cell death also suggests a difference of sensitivity. A similar observation has been made in F9 cells where retinoic acid (RA) induced differentiation of F9 cells into primitive endoderm rescued the apoptosis observed in *Taf10* mutant cells (Metzger et al., 1999). Interestingly, this effect was not observed when F9 cells are differentiated into parietal endoderm in the presence of RA and cAMP (Metzger et al., 1999). One interesting

possibility could be that, being the principal source of RA in the embryo (Niederreither et al., 1997), the paraxial mesoderm is protected from cell death in the mutant embryos via an autocrine mechanism. Another difference of sensitivity has also been made in *Taf10* mutant blastocysts where inner cell mass dies by apoptosis whereas trophoblast can be maintained in culture (Mohan et al., 2003). It is interesting to note that trophoblast, primitive and parietal endoderms are extra-embryonic structures and are not part of the fully-developed embryo. The difference of sensitivity to the loss of *Taf10* in the mesoderm is the first to be observed *in vivo*, in an embryonic lineage. A tempting speculation is that TAF10 could serve as an interface of interaction with a LPM specific transcription factor as it has been described recently for GATA1 during erythropoiesis (Papadopoulos et al., 2015).

Material and Methods

Mice

Animal experimentation was carried out according to animal welfare regulations and guidelines of the French Ministry of Agriculture (ethical committee C2EA-17 projects 2012-077 and 2012-078). All the lines have already been described (see supplementary methods). The day of vaginal plug was scored as embryonic day (E)0.5. Tamoxifen (Sigma) resuspended at 20 mg/ml in 5% EtOH/filtered sunflower seed oil was injected intraperitoneally (150 μl (3 mg) for a 20 g mouse) at E7.5.

Antibodies

Antibodies are listed in the supplementary methods.

Embryos whole cell extracts

E9.5 mouse embryos (16-20 somites) were lysed in 10% glycerol, 20 mM Hepes (pH7), 0.35 M NaCl, 1.5 mM $MgCl_2$, 0.2 mM EDTA, 0.1% Triton X-100 with protease inhibitor cocktail (PIC, Roche) on ice. Lysates were treated 3 times with pestle stroke followed by 3 liquid nitrogen freezing-thaw cycles. Lysates were centrifuged at 20817 rcf for 15 min at 4°C and the supernatants were used directly for IPs or stored at -80°C for western blots.

Immunoprecipitations

Inputs were incubated with Dynabeads coated with antibodies (see supplementary methods) overnight at 4°C. Immunoprecipitated proteins were washed twice 5 min with 500mM KCl buffer (25 mM Tris-HCl (pH7), 5 mM $MgCl_2$, 10% glycerol, 0.1% NP40, 2 mM DTT, 500 mM KCl and PIC (Roche)), then washed twice 5 min with 100 mM KCl buffer (25 mM Tris-

HCl (pH7), 5 mM $MgCl_2$, 10% glycerol, 0.1% NP40, 2 mM DTT, 100 mM KCl and PIC (Roche)) and eluted with 0.1 M glycine (pH2.8) for 5 min three times. Elution fractions were neutralized with 1.5 M Tris-HCl (pH8.8).

Western blots

Immune complexes or 15 μg of embryo lysates were boiled 10 min in 100 mM Tris-pH6.8, 30% glycerol, 4% SDS, 0.2% bromophenol blue, 100 mM DTT, resolved on precast SDS-polyacrylamide gel 4-12% (Novex) and transferred to nitrocellulose membrane (Protran, Amersham). Membranes were blocked in 3% milk in PBS for 30 min and incubated with the primary antibody overnight at 4°C. Membranes were washed three times 5 min with 0.05% Tween20 in PBS. Membranes were incubated with HRP-coupled secondary antibodies for 50 min at RT, followed by ECL detection (ThermoFisher).

Mass spectrometry analyzes

Samples were analyzed using an Ultimate 3000 nano-RSLC (Thermo Scientific, San Jose, California) coupled in line with a linear trap Quadrupole (LTQ)-Orbitrap ELITE mass spectrometer via a nano-electrospray ionization source (Thermo Scientific). Data were analyzed by calculation of the $NSAF_{bait}$ (see supplementary methods).

Section and Immunolocalization

Embryos were fixed in 4% PFA 2 hours at 4°C, rinsed 3 times in PBS, equilibrated in 30% sucrose/PBS and embedded in Cryomatrix (Thermo Scientific) in liquid nitrogen vapours. Twenty μm sections were obtained on a Leica crysotat. Immunolabelling was performed as described (Vincent et al., 2014). Sections were counterstained with DAPI (4',6-diamidino-2-

phenylindole, dihydrochloride, Molecular Probes) and imaged with a LSM 510 laser-scanning microscope (Carl Zeiss MicroImaging) through a 20x Plan APO objective (NA 0.8).

Luvelu imaging

Freshly dissected embryos were kept in DMEM without red phenol (Life technologies). Luvelu signal was detected using a SP5 TCS confocal microscope (Leica) through a 20x Plan APO objective (NA 0.7).

Whole-mount in situ hybridization, X-gal and Lysotracker Red staining

Whole-mount *in situ* hybridizations were performed as described (Nagy et al.). *Axin2*, *Fgf8*, *Hand2*, *Lfng*, *Msgn1*, *Myf5*, *Shh*, *Snai1*and *Uncx4.1* probes have been described (Aulehla and Johnson, 1999; Aulehla et al., 2008; Crossley and Martin, 1995; Dale et al., 2006; Echelard et al., 1993; Mansouri et al., 1997; Ott et al., 1991; Srivastava et al., 1997; Yoon et al., 2000). X-gal and Lysotracker Red (Molecular Probes) stainings were performed as described (Rocancourt et al., 1990; Vincent et al., 2014).

Calculation of the somite index

Somite index was calculated by subtracting the mean of the somite number of a litter from the somite number of each littermate. The somite indexes were then pooled according to the different genotypes. A one-way ANOVA was performed using GraphPad (Prism).

RT-qPCR and statistical analysis

Micro-dissected embryo tail tip or trunk tissue (without limb buds for the controls) were lysed in 500 μl TRIzol (Life technologies). RNA was extracted according to the manufacturer's recommendations and resuspended in 20 μl (trunk) or 11 μl (tail tips) of RNase free water

(Ambion). Reverse transcription was performed using the QuantiTect Reverse Transcription Kit (Qiagen) in 12 μl reaction volume and diluted by adding 75 μl of RNase free water. Quantitative PCRs were performed on a Roche LightCycler II 480 using LightCycler 480 SYBR Green I Master (Roche) in 8 μl reaction (0.4 μl cDNA, 0.5 μM primers). Four mutants and four controls with the same somite number were analysed in triplicates. Statistical analysis and primer sequences are described in the supplementary methods.

Microarrays and statistical analysis

Posterior PSM of E9.5 embryos were individually microdissected (Dequéant et al., 2006) and lysed in 200μl TRIzol (Life technologies), and yolk sac was used for genotyping. Three PSM of 17-19 somites embryos of the same genotype were pooled for one replicate and analysed on GeneChip® MoGene1.0ST (Affymetrix). Data were normalized using RMA (Bioconductor), filtered and FCROS (Dembélé and Kastner, 2014) was used for the statistical analysis (see supplementary methods).

Acknowledgments

We thank Violaine Alumni and the Biochip and Sequencing platform (IGBMC) for the microarray experiments, Doulaye Dembele for his advices on the statistical analysis of the microarrays, Mathilde Decourcelle and the Proteomic platform (IGBMC) for the Orbitrap analyses. We also thank Eli Scheer for her skilful advices on immunoprecipitations, Ivanka Kamenova for her help to validate the antibodies and Joël Herrmann for the validation of the qPCR primers. We thank Didier Devys, Goncalo Vilhais-Neto and Ziad Al Tanoury for their critical reading of the manuscript.

Competing interests

The authors declare no competing or financial interests.

Author contributions

PB performed, interpreted the experiments and contributed to the writing of the manuscript. AH contributed to the imaging and to the *Luvelu* experiments and MF initiated the mass spectrometry analyses. MJ performed the MS analyses. OP and LT funded, contributed to the planning and interpretation of experiments, and contributed to the writing of the manuscript. SDV supervised, planned, performed, interpreted the experiments and wrote the manuscript.

Funding

This work was supported by funds from CNRS, INSERM, Strasbourg University, and Agence Nationale de Recherche (ANR-13-BSV6-0001-02 COREAC; ANR-13-BSV8-0021-03 DiscoverIID to LT), Investissements d'Avenir ANR-10-IDEX-0002-02 (ANR-10-LABX-0030-INRT to LT). LT and OP are recipients of European Research Council (ERC) Advanced grants (ERC-2013-340551, Birtoaction, to LT, and ERC-2009-ADG20090506, Bodybuilt, to OP).

Data availability

Raw microarray data were deposited in GEO database (GSE82186). Raw mass spectrometry data are available via ProteomeXchange with identifier PXD004688.

References

Aulehla, A. and Johnson, R. L. (1999). Dynamic expression of lunatic fringe suggests a link between notch signaling and an autonomous cellular oscillator driving somite segmentation. **207**, 49–61.

Aulehla, A., Wehrle, C., Brand-Saberi, B., Kemler, R., Gossler, A., Kanzler, B. and Herrmann, B. G. (2003). Wnt3a plays a major role in the segmentation clock controlling somitogenesis. *Dev Cell* **4**, 395–406.

Aulehla, A., Wiegraebe, W., Baubet, V., Wahl, M. B., Deng, C., Taketo, M., Lewandoski, M. and Pourquié, O. (2008). A beta-catenin gradient links the clock and wavefront systems in mouse embryo segmentation. *Nat Cell Biol* **10**, 186–193.

Bessho, Y., Hirata, H., Masamizu, Y. and Kageyama, R. (2003). Periodic repression by the bHLH factor Hes7 is an essential mechanism for the somite segmentation clock. *Genes Dev* **17**, 1451–1456.

Bieniossek, C., Papai, G., Schaffitzel, C., Garzoni, F., Chaillet, M., Scheer, E., Papadopoulos, P., Tora, L., Schultz, P. and Berger, I. (2013). The architecture of human general transcription factor TFIID core complex. *Nature* **493**, 699–702.

Bonnet, J., Wang, C.-Y., Baptista, T., Vincent, S. D., Hsiao, W.-C., Stierle, M., Kao, C.-F., Tora, L. and Devys, D. (2014). The SAGA coactivator complex acts on the whole transcribed genome and is required for RNA polymerase II transcription. *Genes Dev* **28**, 1999–2012.

Clements, D., Taylor, H. C., Herrmann, B. G. and Stott, D. (1996). Distinct regulatory control of the Brachyury gene in axial and non-axial mesoderm suggests separation of mesoderm lineages early in mouse gastrulation. *Mech Dev* **56**, 139–149.

Cole, S. E., Levorse, J. M., Tilghman, S. M. and Vogt, T. F. (2002). Clock regulatory elements control cyclic expression of Lunatic fringe during somitogenesis. *Dev Cell* **3**, 75–84.

Crossley, P. H. and Martin, G. R. (1995). The mouse Fgf8 gene encodes a family of polypeptides and is expressed in regions that direct outgrowth and patterning in the developing embryo. *Development* **121**, 439–451.

Dale, J. K., Malapert, P., Chal, J., Vilhais-Neto, G., Maroto, M., Johnson, T., Jayasinghe, S., Trainor, P., Herrmann, B. and Pourquié, O. (2006). Oscillations of the snail genes in the presomitic mesoderm coordinate segmental patterning and morphogenesis in vertebrate somitogenesis. *Dev Cell* **10**, 355–366.

Dembélé, D. and Kastner, P. (2014). Fold change rank ordering statistics: a new method for detecting differentially expressed genes. *BMC Bioinformatics* **15**, 14.

Dequéant, M.-L., Glynn, E., Gaudenz, K., Wahl, M., Chen, J., Mushegian, A. and Pourquié, O. (2006). A complex oscillating network of signaling genes underlies the mouse segmentation clock. *Science* **314**, 1595–1598.

Dulić, V., Kaufmann, W. K., Wilson, S. J., Tlsty, T. D., Lees, E., Harper, J. W., Elledge,

S. J. and Reed, S. I. (1994). p53-dependent inhibition of cyclin-dependent kinase activities in human fibroblasts during radiation-induced G1 arrest. *Cell* **76**, 1013–1023.

Echelard, Y., Epstein, D. J., St-Jacques, B., Shen, L., Mohler, J., McMahon, J. A. and McMahon, A. P. (1993). Sonic hedgehog, a member of a family of putative signaling molecules, is implicated in the regulation of CNS polarity. *Cell* **75**, 1417–1430.

Fernandez-Teran, M., Piedra, M. E., Kathiriya, I. S., Srivastava, D., Rodriguez-Rey, J. C. and Ros, M. A. (2000). Role of dHAND in the anterior-posterior polarization of the limb bud: implications for the Sonic hedgehog pathway. *Development* **127**, 2133–2142.

Forsberg, H., Crozet, F. and Brown, N. A. (1998). Waves of mouse Lunatic fringe expression, in four-hour cycles at two-hour intervals, precede somite boundary formation. *Curr Biol* **8**, 1027–1030.

Gegonne, A., Tai, X., Zhang, J., Wu, G., Zhu, J., Yoshimoto, A., Hanson, J., Cultraro, C., Chen, Q.-R., Guinter, T., et al. (2012). The general transcription factor TAF7 is essential for embryonic development but not essential for the survival or differentiation of mature T cells. *Mol Cell Biol* **32**, 1984–1997.

Goodrich, J. A. and Tjian, R. (2010). Unexpected roles for core promoter recognition factors in cell-type-specific transcription and gene regulation. *Nat Rev Genet* **11**, 549–558.

Goulding, M. D., Chalepakis, G., Deutsch, U., Erselius, J. R. and Gruss, P. (1991). Pax-3, a novel murine DNA binding protein expressed during early neurogenesis. *EMBO J* **10**, 1135–1147.

Gouti, M., Tsakiridis, A., Wymeersch, F. J., Huang, Y., Kleinjung, J., Wilson, V. and Briscoe, J. (2014). In Vitro Generation of Neuromesodermal Progenitors Reveals Distinct Roles for Wnt Signalling in the Specification of Spinal Cord and Paraxial Mesoderm Identity. *PLoS Biol* **12**, e1001937.

Hubaud, A. and Pourquié, O. (2014). Signalling dynamics in vertebrate segmentation. *Nat Rev Mol Cell Biol* **15**, 709–721.

Indra, A. K., Mohan, W. S., Frontini, M., Scheer, E., Messaddeq, N., Metzger, D. and Tora, L. (2005). TAF10 is required for the establishment of skin barrier function in foetal, but not in adult mouse epidermis. **285**, 28–37.

Jacq, X., Brou, C., Lutz, Y., Davidson, I., Chambon, P. and Tora, L. (1994). Human TAFII30 is present in a distinct TFIID complex and is required for transcriptional activation by the estrogen receptor. *Cell* **79**, 107–117.

Kirschner, D. B., Baur, vom, E., Thibault, C., Sanders, S. L., Gangloff, Y.-G., Davidson, I., Weil, P. A. and Tora, L. (2002). Distinct mutations in yeast TAF(II)25 differentially affect the composition of TFIID and SAGA complexes as well as global gene expression patterns. *Mol Cell Biol* **22**, 3178–3193.

Krol, A. J., Roellig, D., Dequéant, M.-L., Tassy, O., Glynn, E., Hattem, G., Mushegian, A., Oates, A. C. and Pourquié, O. (2011). Evolutionary plasticity of segmentation clock networks. *Development* **138**, 2783–2792.

Leurent, C., Sanders, S., Ruhlmann, C., Mallouh, V., Weil, P. A., Kirschner, D. B., Tora, L. and Schultz, P. (2002). Mapping histone fold TAFs within yeast TFIID. *EMBO J* **21**, 3424–3433.

Levine, M., Cattoglio, C. and Tjian, R. (2014). Looping Back to Leap Forward: Transcription Enters a New Era. *Cell* **157**, 13–25.

Lin, Z., Yang, H., Kong, Q., Li, J., Lee, S.-M., Gao, B., Dong, H., Wei, J., Song, J., Zhang, D. D., et al. (2012). USP22 antagonizes p53 transcriptional activation by deubiquitinating Sirt1 to suppress cell apoptosis and is required for mouse embryonic development. *Mol Cell* **46**, 484–494.

Liu, Y., Zhao, J., Zhang, W., Gan, J., Hu, C., Huang, G. and Zhang, Y. (2015). lncRNA GAS5 enhances G1 cell cycle arrest via binding to YBX1 to regulate p21 expression in stomach cancer. *Sci Rep* **5**, 10159.

Ma, C., Shi, X., Zhu, Q., Li, Q., Liu, Y., Yao, Y. and Song, Y. (2015). The growth arrest-specific transcript 5 (GAS5): a pivotal tumor suppressor long noncoding RNA in human cancers. *Tumor Biol*. **37**, 1437–1444.

Mansouri, A., Yokota, Y., Wehr, R., Copeland, N. G., Jenkins, N. A. and Gruss, P. (1997). Paired-related murine homeobox gene expressed in the developing sclerotome, kidney, and nervous system. *Dev Dyn* **210**, 53–65.

McGrew, M. J., Dale, J. K., Fraboulet, S. and Pourquié, O. (1998). The lunatic fringe gene is a target of the molecular clock linked to somite segmentation in avian embryos. *Curr Biol* **8**, 979–982.

Metzger, D., Scheer, E., Soldatov, A. and Tora, L. (1999). Mammalian TAF(II)30 is required for cell cycle progression and specific cellular differentiation programmes. *EMBO J* **18**, 4823–4834.

Mohan, W. S., Scheer, E., Wendling, O., Metzger, D. and Tora, L. (2003). TAF10 (TAF(II)30) is necessary for TFIID stability and early embryogenesis in mice. *Mol Cell Biol* **23**, 4307–4318.

Morales, A. V., Yasuda, Y. and Ish-Horowicz, D. (2002). Periodic Lunatic fringe expression is controlled during segmentation by a cyclic transcriptional enhancer responsive to notch signaling. *Dev Cell* **3**, 63–74.

Müller, F., Zaucker, A. and Tora, L. (2010). Developmental regulation of transcription initiation: more than just changing the actors. *Curr Opin Genet Dev* **20**, 533–540.

Nagy, A., Gertsenstein, M., Vintersten, K. and Behringer, R. R. *Manipulating the Mouse Embryo*. 3rd ed. Cold Spring Harbor: Cold Spring Harbor Laboratory Press.

Neidhardt, L., Kispert, A. and Herrmann, B. (1997). A mouse gene of the paired-related homeobox class expressed in the caudal somite compartment and in the developing vertebral column, kidney and nervous system. *Dev Genes Evol* **207**, 330–339.

Niederreither, K., McCaffery, P., Dräger, U. C., Chambon, P. and Dollé, P. (1997). Restricted expression and retinoic acid-induced downregulation of the retinaldehyde

dehydrogenase type 2 (RALDH-2) gene during mouse development. *Mech Dev* **62**, 67–78.

Niwa, Y., Masamizu, Y., Liu, T., Nakayama, R., Deng, C.-X. and Kageyama, R. (2007). The initiation and propagation of Hes7 oscillation are cooperatively regulated by Fgf and notch signaling in the somite segmentation clock. *Dev Cell* **13**, 298–304.

Ott, M. O., Bober, E., Lyons, G., Arnold, H. and Buckingham, M. (1991). Early expression of the myogenic regulatory gene, myf-5, in precursor cells of skeletal muscle in the mouse embryo. *Development* **111**, 1097–1107.

Papadopoulos, P., Gutiérrez, L., Demmers, J., Scheer, E., Pourfarzad, F., Papageorgiou, D. N., Karkoulia, E., Strouboulis, J., van de Werken, H. J. G., van der Linden, R., et al. (2015). TAF10 Interacts with the GATA1 Transcription Factor and Controls Mouse Erythropoiesis. *Mol Cell Biol* **35**, 2103–2118.

Perantoni, A. O. (2005). Inactivation of FGF8 in early mesoderm reveals an essential role in kidney development. *Development* **132**, 3859–3871.

Pickard, M. and Williams, G. (2015). Molecular and Cellular Mechanisms of Action of Tumour Suppressor GAS5 LncRNA. *Genes* **6**, 484–499.

Pourquié, O. (2011). Vertebrate segmentation: from cyclic gene networks to scoliosis. *Cell* **145**, 650–663.

Rocancourt, D., Bonnerot, C., Jouin, H., Emerman, M. and Nicolas, J. F. (1990). Activation of a beta-galactosidase recombinant provirus: application to titration of human immunodeficiency virus (HIV) and HIV-infected cells. *J Virol* **64**, 2660–2668.

Saga, Y., Hata, N., Koseki, H. and Taketo, M. M. (1997). Mesp2: a novel mouse gene expressed in the presegmented mesoderm and essential for segmentation initiation. *Genes Dev* **11**, 1827–1839.

Sainsbury, S., Bernecky, C. and Cramer, P. (2015). Structural basis of transcription initiation by RNA polymerase II. *Nat Rev Mol Cell Biol* **16**, 129–143.

Sapountzi, V. and Côté, J. (2011). MYST-family histone acetyltransferases: beyond chromatin. *Cell Mol Life Sci* **68**, 1147–1156.

Soriano, P. (1999). Generalized lacZ expression with the ROSA26 Cre reporter strain. *Nat Genet* **21**, 70–71.

Soutoglou, E., Demény, M. A., Scheer, E., Fienga, G., Sassone-Corsi, P. and Tora, L. (2005). The nuclear import of TAF10 is regulated by one of its three histone fold domain-containing interaction partners. *Mol Cell Biol* **25**, 4092–4104.

Spedale, G., Timmers, H. T. M. and Pijnappel, W. W. M. P. (2012). ATAC-king the complexity of SAGA during evolution. *Genes Dev* **26**, 527–541.

Srivastava, D., Thomas, T., Lin, Q., Kirby, M. L., Brown, D. and Olson, E. N. (1997). Regulation of cardiac mesodermal and neural crest development by the bHLH transcription factor, dHAND. *Nat Genet* **16**, 154–160.

Tatarakis, A., Margaritis, T., Martinez-Jimenez, C. P., Kouskouti, A., Mohan, W. S., Haroniti, A., Kafetzopoulos, D., Tora, L. and Talianidis, I. (2008). Dominant and redundant functions of TFIID involved in the regulation of hepatic genes. *Mol Cell* **31**, 531–543.

Timmers, H. T. and Sharp, P. A. (1991). The mammalian TFIID protein is present in two functionally distinct complexes. *Genes Dev* **5**, 1946–1956.

Trowitzsch, S., Viola, C., Scheer, E., Conic, S., Chavant, V., Fournier, M., Papai, G., Ebong, I.-O., Schaffitzel, C., Zou, J., et al. (2015). Cytoplasmic TAF2-TAF8-TAF10 complex provides evidence for nuclear holo-TFIID assembly from preformed submodules. *Nat Commun* **6**, 6011.

Tzouanacou, E., Wegener, A., Wymeersch, F. J., Wilson, V. and Nicolas, J.-F. (2009). Redefining the progression of lineage segregations during mammalian embryogenesis by clonal analysis. *Dev Cell* **17**, 365–376.

Vannini, A. and Cramer, P. (2012). Conservation between the RNA polymerase I, II, and III transcription initiation machineries. *Mol Cell* **45**, 439–446.

Ventura, A., Kirsch, D. G., McLaughlin, M. E., Tuveson, D. A., Grimm, J., Lintault, L., Newman, J., Reczek, E. E., Weissleder, R. and Jacks, T. (2007). Restoration of p53 function leads to tumour regression in vivo. *Nature* **445**, 661–665.

Vincent, S. D., Dunn, N. R., Sciammas, R., Shapiro-Shalef, M., Davis, M. M., Calame, K., Bikoff, E. K. and Robertson, E. J. (2005). The zinc finger transcriptional repressor Blimp1/Prdm1 is dispensable for early axis formation but is required for specification of primordial germ cells in the mouse. *Development* **132**, 1315–1325.

Vincent, S. D., Mayeuf-Louchart, A., Watanabe, Y., Brzezinski, J. A., Miyagawa-Tomita, S., Kelly, R. G. and Buckingham, M. (2014). Prdm1 functions in the mesoderm of the second heart field, where it interacts genetically with Tbx1, during outflow tract morphogenesis in the mouse embryo. *Hum Mol Genet* ddu232.

Voss, A. K., Thomas, T., Petrou, P., Anastassiadis, K., Schöler, H. and Gruss, P. (2000). Taube nuss is a novel gene essential for the survival of pluripotent cells of early mouse embryos. *Development* **127**, 5449–5461.

Wang, L. and Dent, S. Y. R. (2014). Functions of SAGA in development and disease. *Epigenomics* **6**, 329–339.

Weake, V. M., Dyer, J. O., Seidel, C., Box, A., Swanson, S. K., Peak, A., Florens, L., Washburn, M. P., Abmayr, S. M. and Workman, J. L. (2011). Post-transcription initiation function of the ubiquitous SAGA complex in tissue-specific gene activation. *Genes Dev* **25**, 1499–1509.

Wittler, L., Shin, E.-H., Grote, P., Kispert, A., Beckers, A., Gossler, A., Werber, M. and Herrmann, B. G. (2007). Expression of Msgn1 in the presomitic mesoderm is controlled by synergism of WNT signalling and Tbx6. *EMBO Rep* **8**, 784–789.

Xu, W., Edmondson, D. G., Evrard, Y. A., Wakamiya, M., Behringer, R. R. and Roth, S. Y. (2000). Loss of Gcn5l2 leads to increased apoptosis and mesodermal defects during

mouse development. *Nat Genet* **26**, 229–232.

Yamauchi, T., Yamauchi, J., Kuwata, T., Tamura, T., Yamashita, T., Bae, N., Westphal, H., Ozato, K. and Nakatani, Y. (2000). Distinct but overlapping roles of histone acetylase PCAF and of the closely related PCAF-B/GCN5 in mouse embryogenesis. *Proc Natl Acad Sci USA* **97**, 11303–11306.

Yoon, J. K., Moon, R. T. and Wold, B. (2000). The bHLH class protein pMesogenin1 can specify paraxial mesoderm phenotypes. **222**, 376–391.

Zeller, R., López-Ríos, J. and Zuniga, A. (2009). Vertebrate limb bud development: moving towards integrative analysis of organogenesis. *Nat Rev Genet* **10**, 845–858.

Zhou, H., Grubisic, I., Zheng, K., He, Y., Wang, P. J., Kaplan, T. and Tjian, R. (2013a). Taf7l cooperates with Trf2 to regulate spermiogenesis. *PNAS* **110**, 16886–16891.

Zhou, H., Kaplan, T., Li, Y., Grubisic, I., Zhang, Z., Wang, P. J., Eisen, M. B. and Tjian, R. (2013b). Dual functions of TAF7L in adipocyte differentiation. *Elife* **2**, e00170.

Zybailov, B., Mosley, A. L., Sardiu, M. E., Coleman, M. K., Florens, L. and Washburn, M. P. (2006). Statistical analysis of membrane proteome expression changes in Saccharomyces cerevisiae. *J. Proteome Res.* **5**, 2339–2347.

description	symbol	absolute FC	f value
cell cycle			
growth arrest specific 5	*Gas5*	-4.9075408	0.017718801
growth arrest specific 5	*Gas5*	-3.736196532	0.017771121
growth arrest specific 5	*Gas5*	-2.634510323	0.017886397
growth arrest specific 5	*Gas5*	-2.072799706	0.018319525
cyclin-dependent kinase inhibitor 1A (P21)	*Cdkn1a*	4.789628182	0.982045384
cyclin-dependent kinase inhibitor 1C (P57)	*Cdkn1c*	1.525180853	0.979478088
cyclin-dependent kinase-like 3	*Cdkl3*	1.779798823	0.981084679
cyclin G1	*Ccng1*	2.005804019	0.981733355
RNA pol I associated complexes			
TATA box binding protein (Tbp)-associated factor, RNA polymerase I, D	*Taf1d*	-2.317074936	0.018087818
TATA box binding protein (Tbp)-associated factor, RNA polymerase I, D	*Taf1d*	-2.266286542	0.01809225
TATA box binding protein (Tbp)-associated factor, RNA polymerase I, D	*Taf1d*	-2.039738816	0.018555265
TATA box binding protein (Tbp)-associated factor, RNA polymerase I, D	*Taf1d*	-1.785722753	0.019331127
TATA box binding protein (Tbp)-associated factor, RNA polymerase I, D	*Taf1d*	-1.632420432	0.020404534
RNA pol II associated complexes			
TAF6 RNA polymerase II, TATA box binding protein (TBP)-associated factor	*Taf6*	1.72440928	0.980946134
TAF9B RNA polymerase II, TATA box binding protein (TBP)-associated factor	*Taf9b*	1.591031326	0.978636615
TAF5 RNA polymerase II, TATA box binding protein (TBP)-associated factor	*Taf5*	1.536439612	0.978826464
polymerase (RNA) II (DNA directed) polypeptide A	*Polr2a*	1.5052891	0.979153598
signaling pathways and transcription factors			
Mix1 homeobox-like 1 (Xenopus laevis)	*Mixl1*	1.565820524	0.97874697
T-box 6	*Tbx6*	1.546625984	0.979948731
E26 avian leukemia oncogene 2, 3' domain	*Ets2*	-1.537617023	0.021680906
fibroblast growth factor 9	*Fgf9*	-1.549855417	0.02153317
ephrin A5	*Efna5*	-1.627750959	0.020793883
dual specificity phosphatase 4	*Dusp4*	-1.647697371	0.02022193
R-spondin 3 homolog (Xenopus laevis)	*Rspo3*	-1.661619669	0.020011719
cytochrome P450, family 26, subfamily a, polypeptide 1	*Cyp26a1*	-1.671145052	0.020601729
caudal type homeobox 4	*Cdx4*	-1.51866511	0.023200463
homeobox A7	*Hoxa7*	1.635575113	0.980606968
homeobox B7	*Hoxb7*	1.822569059	0.981446929
homeobox D1	*Hoxd1*	1.97112032	0.981663225
homeobox A3	*Hoxa3*	2.549458032	0.981967438
cyclic genes			
early growth response 1	*Egr1*	1.610151831	0.979126918
cysteine rich protein 61	*Cyr61*	1.713059121	0.981037055
dickkopf homolog 1 (Xenopus laevis)	*Dkk1*	1.944872688	0.981052429
sprouty homolog 4 (Drosophila)	*Spry4*	-1.538775581	0.021864177
ribosomal protein S3A	*Rps3a*	-1.585508682	0.020915584

Table 1. Selection of differentially expressed genes in the PSM of E9.5 *T-Cre;Taf10* mutant embryos. The statistical analysis has been performed using FCROS with a cut-off of 1.5 for the fold change. Difference is considered significant for a f value below 0.025 or above 0.975.

Legend to Figures

Fig. 1. Efficient ubiquitous deletion of *Taf10* in E9.5 *R26Cre*;*Taf10* mutant embryos. (A-F) Whole-mount Xgal staining of E9.5 *R26*$^{CreERT2/R}$;*Taf10*$^{flox/+}$ (A) or E10.5 (C) and E11.5 (E) *R26*$^{+/R}$;*Taf10*$^{flox/flox}$ control embryos and E9.5 (B), E10.5 (D) and E11.5 (F) *R26*$^{CreERT2/R}$;*Taf10*$^{flox/flox}$ mutant embryos after tamoxifen treatment at E7.5 (+tam). (G) Western blot analysis of 4 E9.5 *R26Cre*;*Taf10* whole embryo treated (+) or not (-) with tamoxifen at E7.5 with anti-TAF10 (top) and anti-H3 (bottom) antibodies. (H-I) Confocal z-stack images projection of E9.25 *R26*$^{CreERT2/+}$;*Taf10*$^{flox/flox}$;*Luvelu*/+ non treated (H) or treated (I) embryos with tamoxifen (+tam). Scale bars in A-F and H-I represent 500 μm, and 100 μm, respectively tam; tamoxifen.

Fig. 2. Assembly defect of the TFIID complex in *R26Cre;Taf10* mutant embryos. (A) Western blot analysis of the expression of TBP, TAF4A, TAF5, TAF6, TAF8 and TAF10 from whole cell lysates of E9.5 *R26Cre;Taf10* embryos control (left, untreated) or mutant (right, treated with tamoxifen at E7.5) (B) $NSAF_{bait}$ values for SL1 complex subunits (TAF1A, TAF1B, TAF1C, TAF1D and TBP) and TF3B-TBP complex of TBP. (C-D) $NSAF_{bait}$ values for TFIID subunits of TBP (C) and TAF7 (D) IPs. The bait proteins are indicated in red. The control and mutant IPs are indicated in white and grey, respectively. TAF10* corresponds to the full-lengthTAF10 protein. tam; tamoxifen

Fig. 3. Assembly defect of the SAGA complex in *R26Cre;Taf10* mutant embryos. (A) $NSAF_{bait}$ values for TIP60/NuA4 complex subunits of TRRAP IP from control (white) and mutant (grey) extracts. (B-C) $NSAF_{bait}$ values for SAGA subunits of TRRAP (C) and SUPT3

(D) IPs from control (white) and mutant (grey) extracts. The bait proteins are indicated in red. TAF10* corresponds to the full-length TAF10 protein.

Fig. 4. Efficient *Taf10* conditional deletion *Taf10* in the paraxial mesoderm. (A-C) Whole-mount right sided view of control (A,C) and *T-Cre;Taf10* mutant (B,D) embryos at E9.25 (A,B) and E10.25 (C,D). The arrowhead in C,D indicates the position of the forelimb bud that is absent in the mutant, the arrow indicates the somites. (E,F) Cell death assay by LysoTracker Red staining of E9.25 control (E) and *T-Cre;Taf10* mutant (F) embryos. (G,H) Whole-mount X gal stained E8.75 *T-Cre*/+;*R26*$^{R/+}$ control (G) and *T-Cre*/+;*R26*$^{R/+}$;*Taf10*$^{flox/flox}$ mutant (H) embryos showing the efficient early recombination within the paraxial mesoderm. (I-L) DAPI counterstained TAF10 immunolocalization on sagittal (I,J) and transverse (K,L) sections from E9.5 (I,J) and E9.75 (K,L) control (I,K) and *T-Cre;Taf10* mutant (J,L) embryos. so; somites, PSM; presomitic mesoderm, NT; neural tube, Ec; ectoderm, Pm; paraxial mesoderm. The asterisk (*) in (K,L) indicates background due to the trapping of the secondary antibody in the endoderm lumen. Scale bars in A-H and I-L represent 500 μm and 50 μm, respectively.

Fig. 5. Segmentation is not affected in absence of TAF10 in the PSM. (A) Quantification of the somite index (one-way ANOVA, ns; non significant). The error bars indicate the s.e.m. and the middle bar indicates the mean. (B-I) Whole-mount *in situ* hybridization of E9.5 (B,C,F,G,H,I) and E8.75 (D,E) control (B,D,F,H) and *T-Cre*/+;*Taf10*$^{flox/flox}$ mutant (C,E,G,I) embryos using posterior PSM marker *Msgn1* (B,C), clock target *Mesp2* (D,E) and caudal somite marker *Uncx4.1* (F,G) and cyclic gene *Lfng* (H,I) probes. Dorsal tail tip (B-E,H,I) or right-lateral views (F,G) are presented. Scale bars in B-E,H-I and F-G represent 100 μm and 500 μm, respectively.

Fig. 6. Absence of TAF10 differentially affects the different types of mesoderm. (A-F) DAPI staining on transversal sections of E10.25 control (A, magnifications in C,E) and *T-Cre*/+;*Taf10*$^{flox/flox}$ mutant (B, magnifications in D,F) embryos showing nuclear fragmentation in LPM but normal nuclear morphology in the paraxial mesoderm. (G-P) Whole-mount *in situ* hybridization of E9.5 control (G,I,K,M,O) and *T-Cre*/+;*Taf10*$^{flox/flox}$ mutant (H,J,L,N,P) embryos using *Hand2* (G,H), *Pax3* (I,J), *Myf5* (K,L), *Fgf8* (M,N) and *Shh* (O,P). The arrow in M,N indicates the Apical Ectodermal Ridge. Pm; paraxial mesoderm, LPM; lateral plate mesoderm, the asterisks (*) in D and E indicate the endoderm. Scale bars in A-F and G-P represent 50 μm and 500 μm, respectively.

Fig. 7. Global transcription is not affected in absence of TAF10 in the paraxial mesoderm. (A) Scheme of the comparison between RNA polymerase II (Pol II) and RNA polymerase I (Pol I) transcription. Trunk axial structures highlighted in blue were dissected from E9.75 control and *T-Cre*/+;*Taf10*$^{flox/flox}$ mutant embryos and RT-qPCR was performed for Pol I and Pol II specific house keeping genes. (B) Comparison of averaged and normalized expression of Pol I (blue) and Pol II (red) specific markers from control (white) and mutant (grey) samples. **; p-value <0.01 (n=4, Aspin Welch corrected Student's *t*-test). The error bars indicate s.e.m. (C,D) Confocal z-stack images projection of E9.5 *Luvelu*/+ control (C) and *T-Cre*/+;*Taf10*$^{flox/flox}$;*Luvelu*/+ mutant (D). Scale bars in C-D represent 100 μm.

Fig. 8. Limited specific effect on RNA polymerase II transcription in absence of TAF10 in the PSM. (A) Scheme of the strategy used for the microarray analysis. E9.5 microdissected PSM of control (blue) and *T-Cre*;*Taf10* mutant (red) embryos were used as source of material. (B) Scatter plot comparing gene expression between control and *T-Cre*;*Taf10* mutant PSM.

Red dots correspond to statistically significant differences for a fold change greater than 1.5 after a *t*-test. (C) Vulcano plot comparing gene expression between control and *T-Cre*/+;*Taf10*$^{flox/flox}$ mutant PSM after a FCROS analysis. Red dots correspond to statistically significant differences for a fold change greater than 1.5. (D) RT-qPCR analysis for cell-cycle genes candidates from E9.25 control (white) and *TCre*;*Taf10* mutant (grey) tail tips: -ΔΔCp are normalized to *Gapdh*. ns; non significant, *; p-value <0.05, **; p-value <0.01, ***; p-value <0.001 (n=4, Aspin Welch corrected Student's *t*-test). The error bars indicate s.e.m.

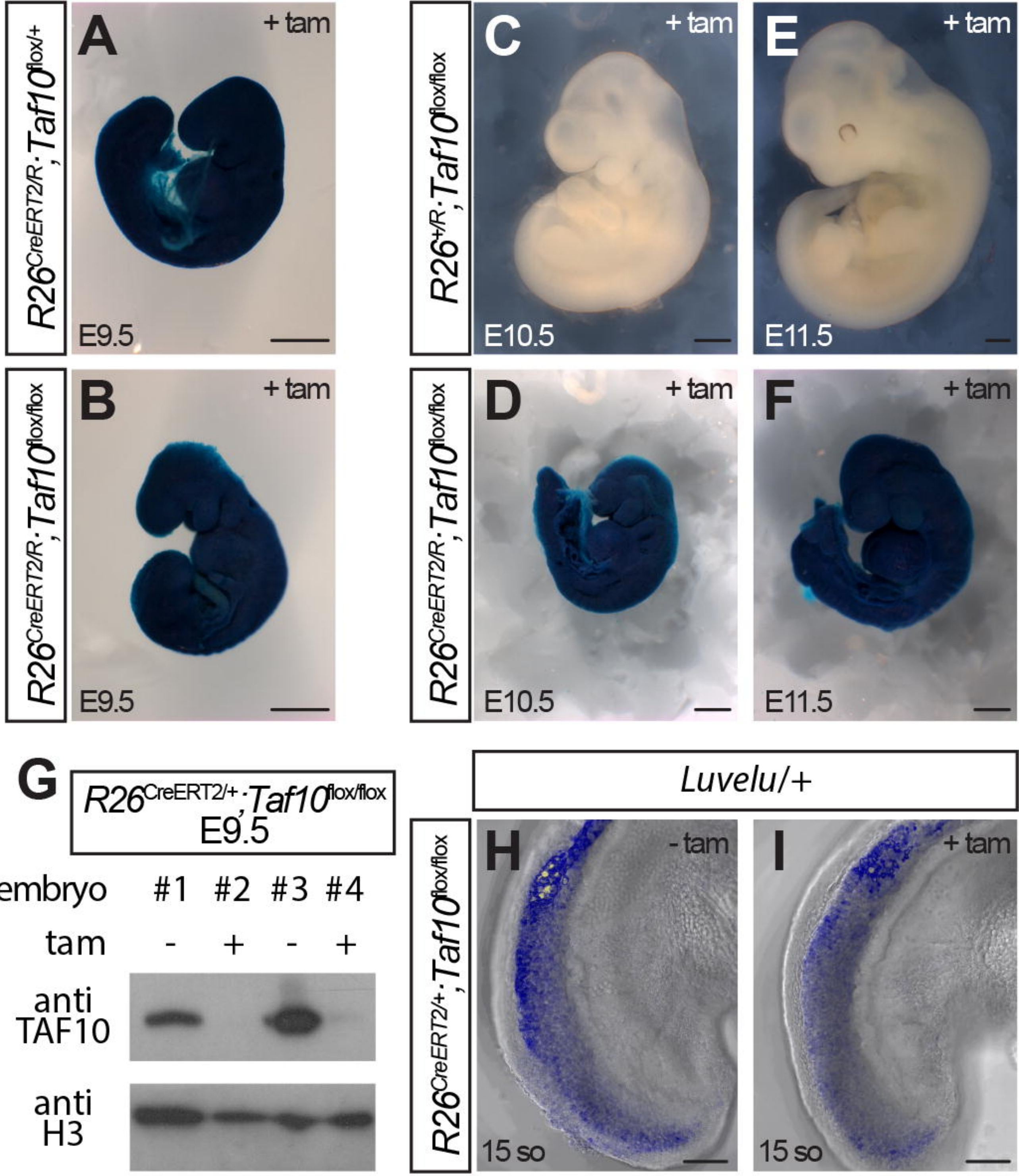
R26CreERT2/R;Taf10flox/+
A
+ tam
E9.5
R26CreERT2/R;Taf10flox/flox
B
+ tam
E9.5
R26+/R;Taf10flox/flox
C
+ tam
E10.5
R26CreERT2/R;Taf10flox/flox
D
+ tam
E10.5
E
+ tam
E11.5
F
+ tam
E11.5
G
R26CreERT2/+;Taf10flox/flox
E9.5
embryo #1 #2 #3 #4
tam - + - +
anti TAF10
anti H3
Luvelu/+
R26CreERT2/+;Taf10flox/flox
H
- tam
15 so
I
+ tam
15 so

Figure 1

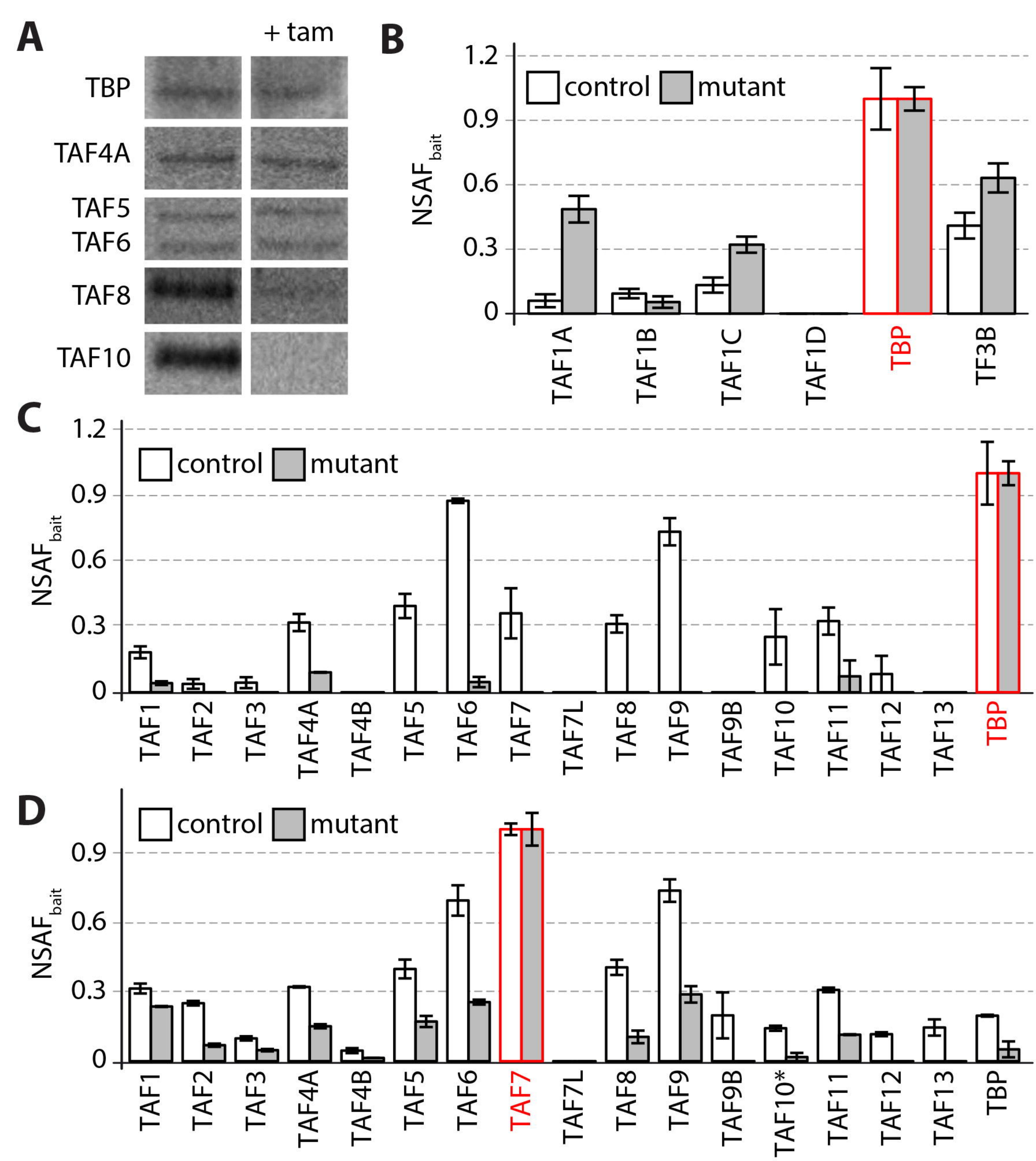
A
+ tam
TBP
TAF4A
TAF5
TAF6
TAF8
TAF10
B
control
mutant
NSAF bait
1.2
0.9
0.6
0.3
0
TAF1A
TAF1B
TAF1C
TAF1D
TBP
TF3B
C
control
mutant
NSAF bait
1.2
0.9
0.6
0.3
0
TAF1
TAF2
TAF3
TAF4A
TAF4B
TAF5
TAF6
TAF7
TAF7L
TAF8
TAF9
TAF9B
TAF10
TAF11
TAF12
TAF13
TBP
D
control
mutant
NSAF bait
0.9
0.6
0.3
0
TAF1
TAF2
TAF3
TAF4A
TAF4B
TAF5
TAF6
TAF7
TAF7L
TAF8
TAF9
TAF9B
TAF10*
TAF11
TAF12
TAF13
TBP

Figure 2

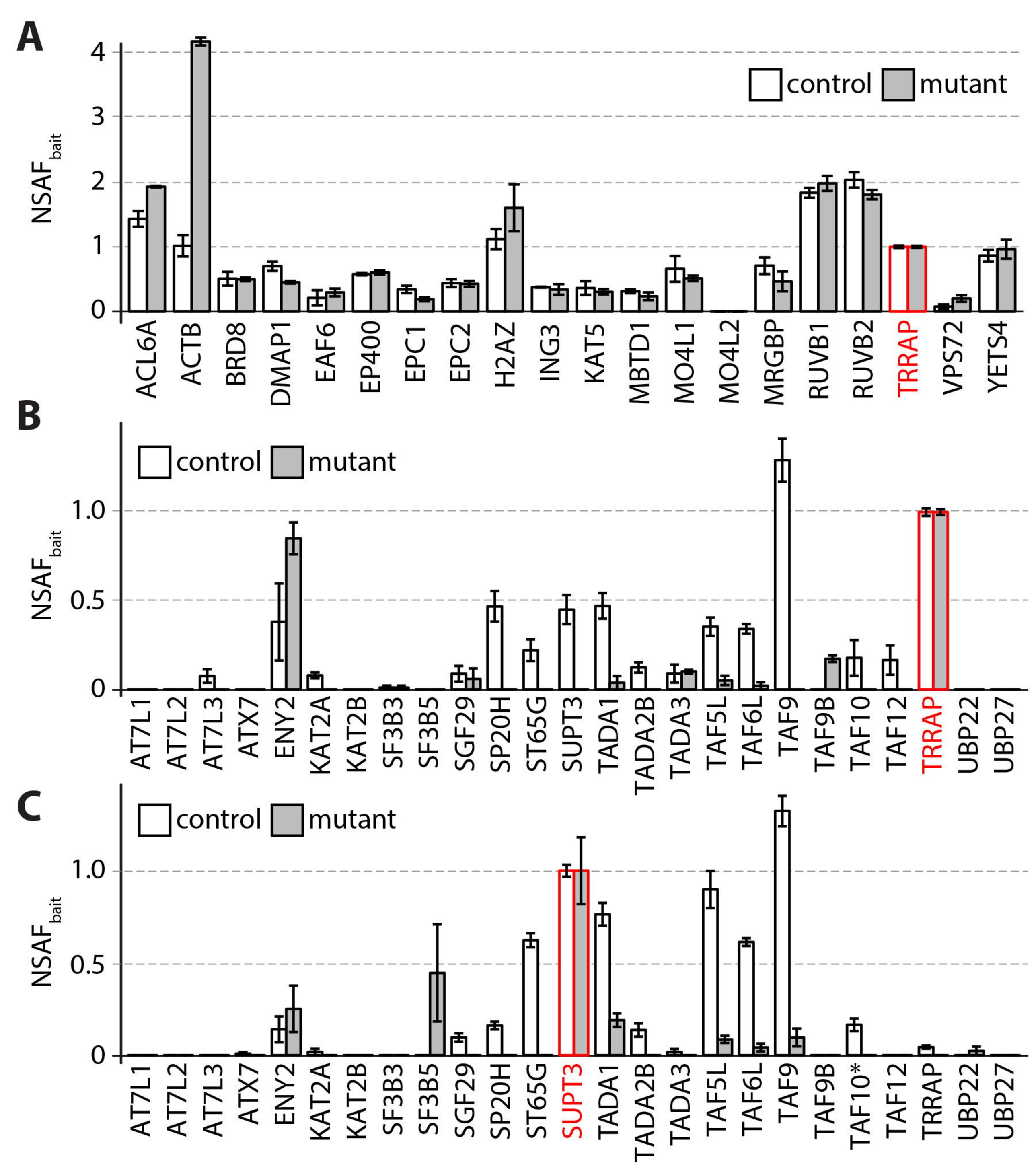
A
control
mutant
NSAF bait
4
3
2
1
0
ACL6A
ACTB
BRD8
DMAP1
EAF6
EP400
EPC1
EPC2
H2AZ
ING3
KAT5
MBTD1
MO4L1
MO4L2
MRGBP
RUVB1
RUVB2
TRRAP
VPS72
YETS4
B
control
mutant
NSAF bait
1.0
0.5
0
AT7L1
AT7L2
AT7L3
ATX7
ENY2
KAT2A
KAT2B
SF3B3
SF3B5
SGF29
SP20H
ST65G
SUPT3
TADA1
TADA2B
TADA3
TAF5L
TAF6L
TAF9
TAF9B
TAF10
TAF12
TRRAP
UBP22
UBP27
C
control
mutant
NSAF bait
1.0
0.5
0
AT7L1
AT7L2
AT7L3
ATX7
ENY2
KAT2A
KAT2B
SF3B3
SF3B5
SGF29
SP20H
ST65G
SUPT3
TADA1
TADA2B
TADA3
TAF5L
TAF6L
TAF9
TAF9B
TAF10*
TAF12
TRRAP
UBP22
UBP27

Figure 3

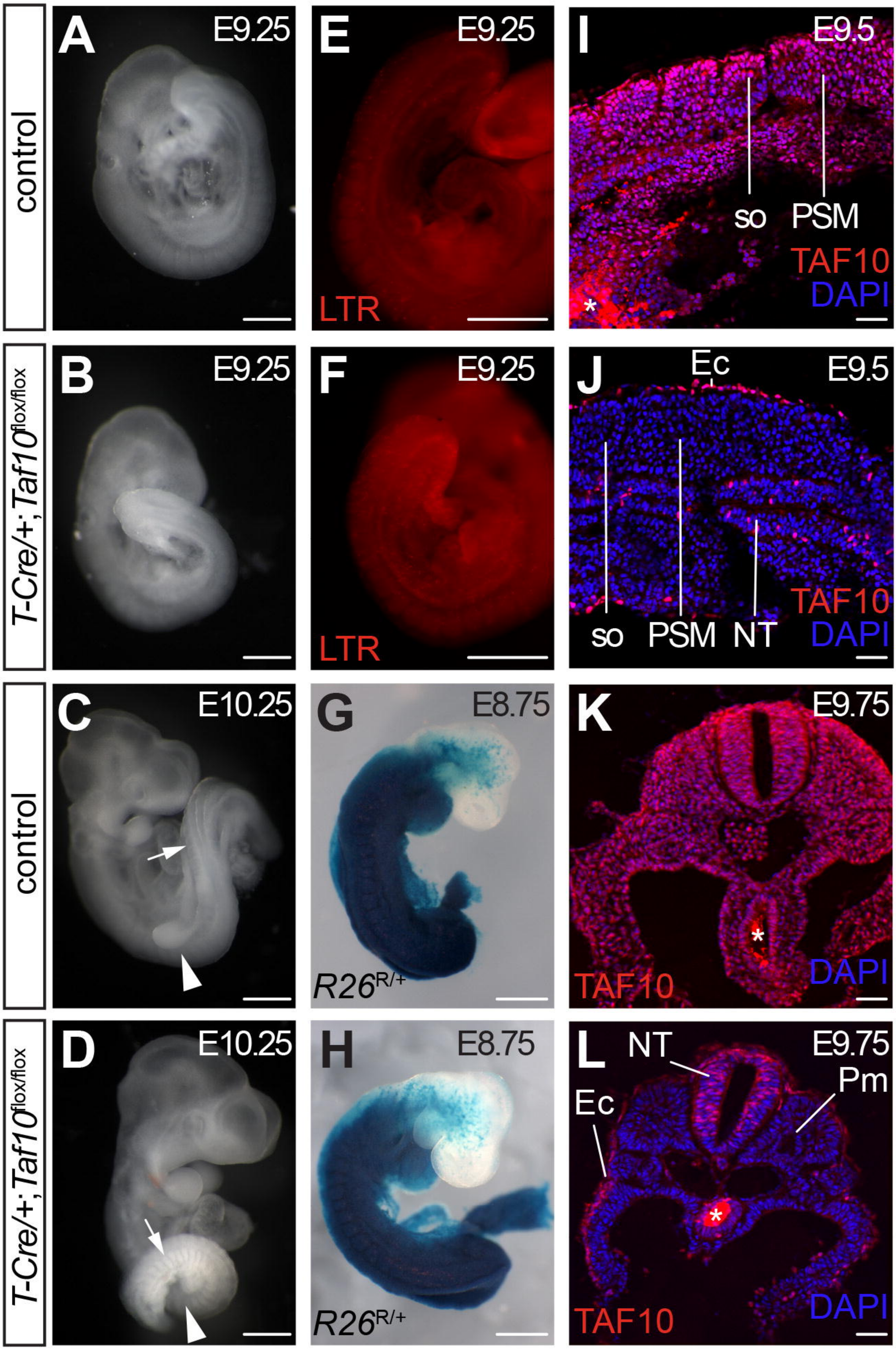
control
T-Cre/+; Taf10flox/flox
control
T-Cre/+; Taf10flox/flox
A
E9.25
B
E9.25
C
E10.25
D
E10.25
E
E9.25
LTR
F
E9.25
LTR
G
E8.75
R26R/+
H
E8.75
R26R/+
I
E9.5
so
PSM
TAF10
DAPI
*
J
Ec
E9.5
so
PSM
NT
TAF10
DAPI
K
E9.75
*
TAF10
DAPI
L
NT
E9.75
Pm
Ec
*
TAF10
DAPI

Figure 4

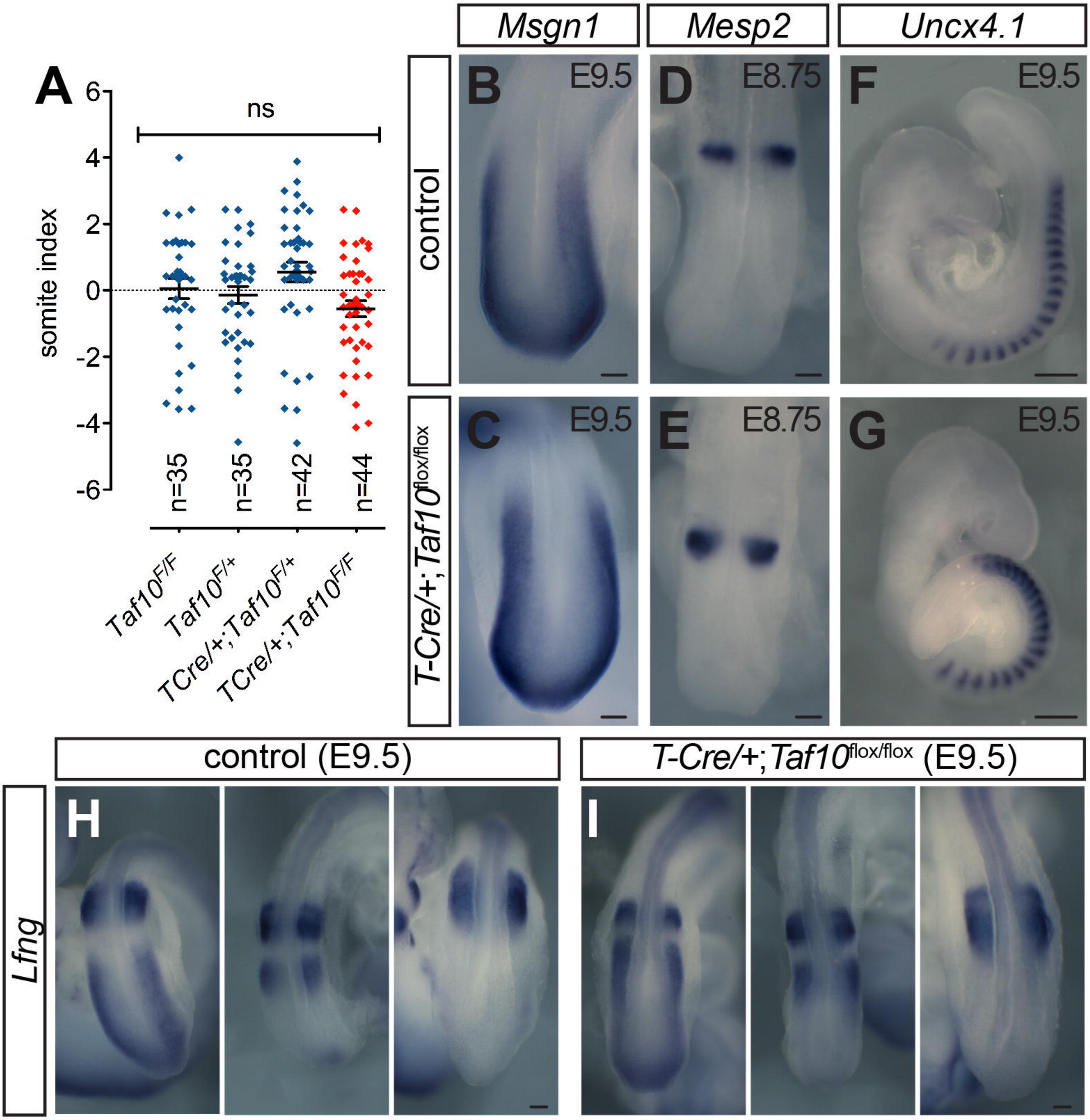
A
ns
somite index
6
4
2
0
-2
-4
-6
n=35
n=35
n=42
n=44
Taf10F/F
Taf10F/+
TCre/+;Taf10F/+
TCre/+;Taf10F/F
Msgn1
Mesp2
Uncx4.1
control
T-Cre/+;Taf10flox/flox
B E9.5
D E8.75
F E9.5
C E9.5
E E8.75
G E9.5
control (E9.5)
T-Cre/+;Taf10flox/flox (E9.5)
Lfng
H
I

Figure 5

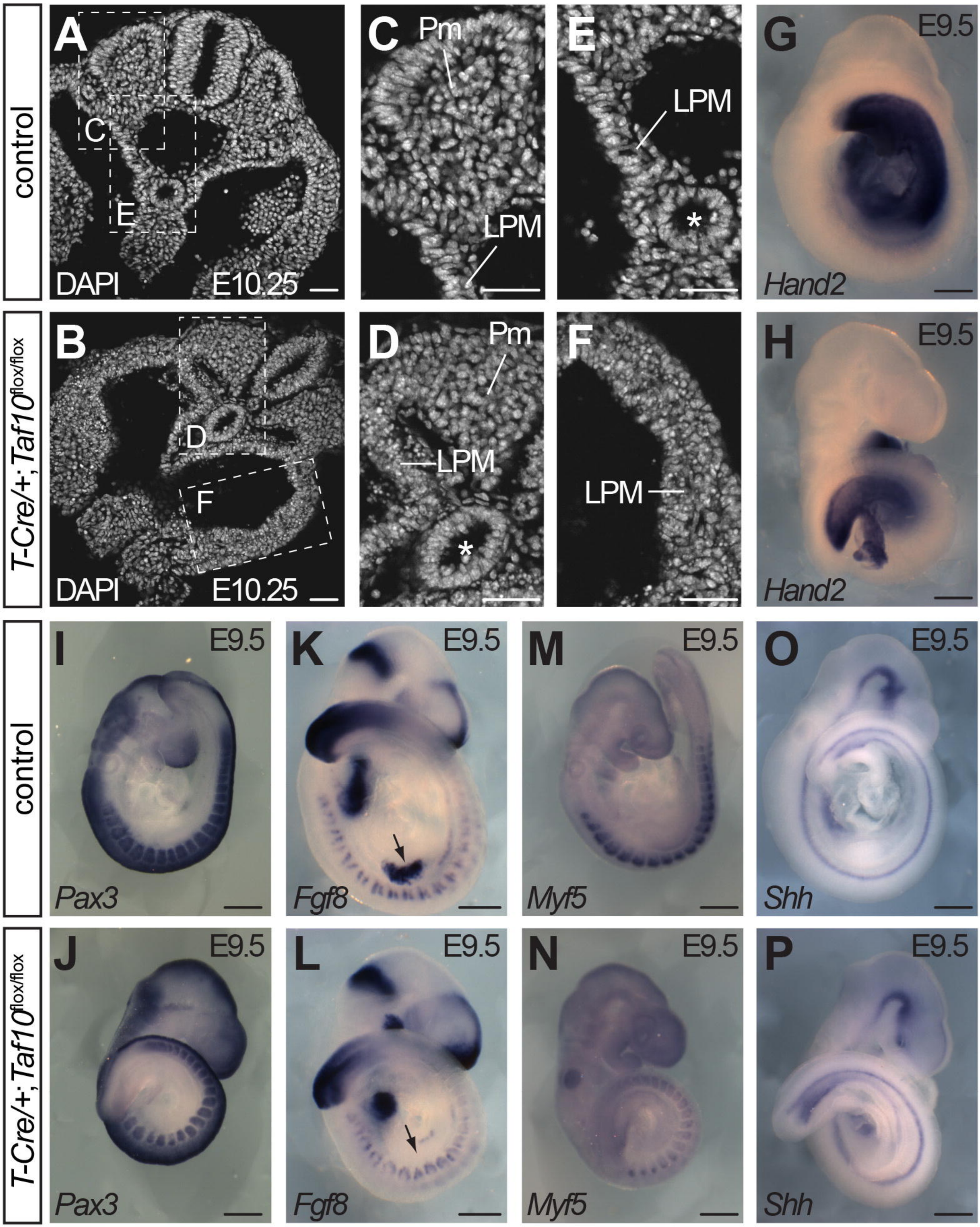
control
T-Cre/+; Taf10flox/flox
A
C
E
DAPI
E10.25
B
D
F
DAPI
E10.25
C
Pm
LPM
D
Pm
LPM
*
E
LPM
*
F
LPM
G
E9.5
Hand2
H
E9.5
Hand2
I
E9.5
Pax3
K
E9.5
Fgf8
M
E9.5
Myf5
O
E9.5
Shh
J
E9.5
Pax3
L
E9.5
Fgf8
N
E9.5
Myf5
P
E9.5
Shh

Figure 6

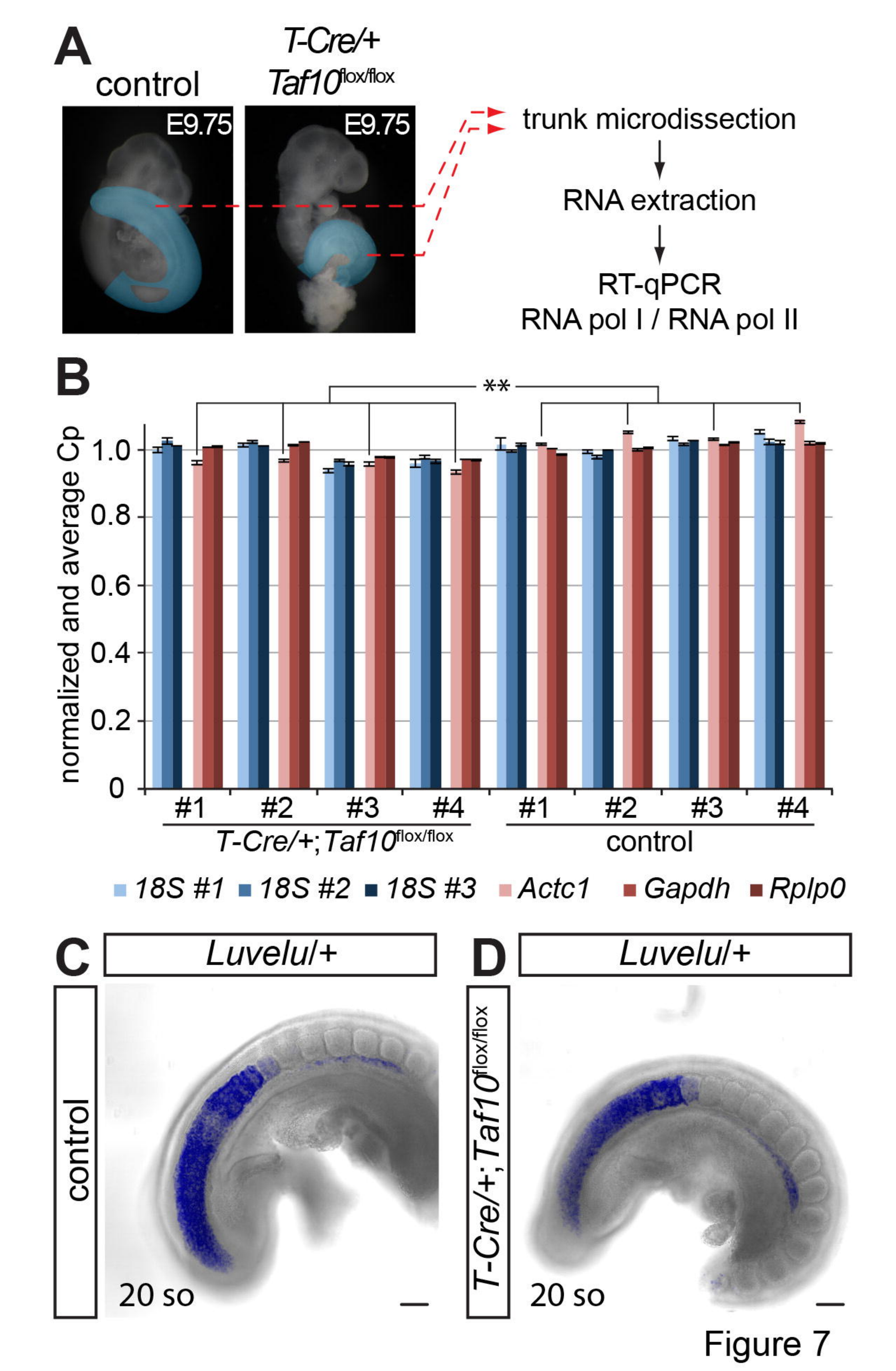
A
control
T-Cre/+
Taf10flox/flox
E9.75
E9.75
trunk microdissection
RNA extraction
RT-qPCR
RNA pol I / RNA pol II
B
**
normalized and average Cp
1.0
0.8
0.6
0.4
0.2
0
#1
#2
#3
#4
#1
#2
#3
#4
T-Cre/+;Taf10flox/flox
control
18S #1
18S #2
18S #3
Actc1
Gapdh
Rplp0
C
Luvelu/+
control
20 so
D
Luvelu/+
T-Cre/+;Taf10flox/flox
20 so

Figure 7

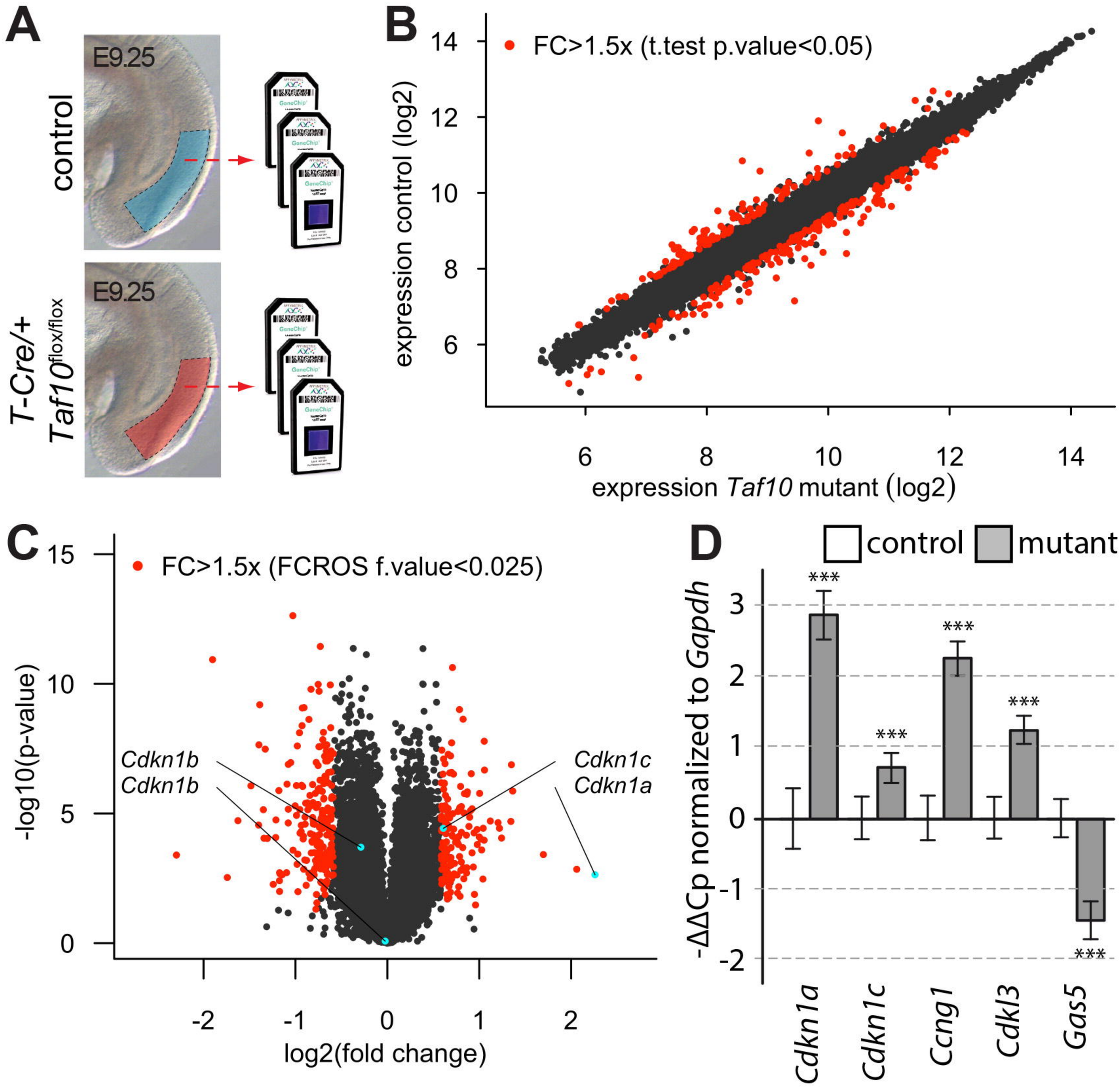
A
E9.25
control
E9.25
T-Cre/+
Taf10flox/flox
B
FC>1.5x (t.test p.value<0.05)
expression control (log2)
expression Taf10 mutant (log2)
C
FC>1.5x (FCROS f.value<0.025)
-log10(p-value)
log2(fold change)
Cdkn1b
Cdkn1b
Cdkn1c
Cdkn1a
D
control
mutant
-ΔΔCp normalized to Gapdh
Cdkn1a
Cdkn1c
Ccng1
Cdkl3
Gas5

Figure 8